

R. & M. No. 3537



LIBRARY
ROYAL AIRCRAFT ESTABLISHMENT
BEDFORD.

MINISTRY OF TECHNOLOGY

AERONAUTICAL RESEARCH COUNCIL
REPORTS AND MEMORANDA

Measurements in a Three-dimensional Turbulent
Boundary Layer in Supersonic Flow

By M. G. Hall and H. B. Dickens

LONDON: HER MAJESTY'S STATIONERY OFFICE

1968

PRICE £1 2s. 6d. NET

Measurements in a Three-dimensional Turbulent Boundary Layer in Supersonic Flow

By M. G. Hall and H. B. Dickens

*Reports and Memoranda No. 3537**

July, 1966

Summary.

In this Report the details are given of the results of measurements of mean values in time of pitot pressure and flow direction made in the boundary layer over the insulated side-wall of a specially constructed supersonic nozzle. The external flow first accelerated and then decelerated, and the crosswise pressure gradients were such that the boundary-layer cross-flow was first in one direction and then in the opposite, as happens over wings with swept leading edges. The external Mach number ranged between 1.6 and 2.0. Boundary-layer traverses were made at intervals along external streamlines; from each traverse, profiles of Mach number and streamwise and cross-wise components of velocity were derived. The results were supplemented by measurements of skin friction using surface tubes, and displacement and momentum thicknesses were evaluated.

All the results are presented in tabular form, and a discussion is given in which serious limitations in the commonly assumed forms for the cross-flow profiles are pointed out. There is evidence, however, that the streamwise component behaves as it would in an equivalent two-dimensional boundary layer.

CONTENTS

1. Introduction
2. Experimental Apparatus
3. Experimental Procedure
4. The Processing of Observations and Presentation of Results
5. Discussion of the Results
 - 5.1. Profiles of cross-flow
 - 5.2. Streamwise flow
 - 5.3. Momentum integral equations
 - 5.4. Concluding remarks

*Replaces R.A.E. Tech. Report No. 66 214—A.R.C. 28 599.

List of Symbols

References

Table 1 Ordinates of external streamlines and liners

Table 2 Static-pressure distribution over wall

Table 3 Boundary-layer profiles

Table 4 Displacement and momentum thicknesses in inches, and the ratio H_i

Table 5 Estimates of skin-friction coefficient

Table 6 Curvatures of streamline and orthogonals

Illustrations—Figs. 1 to 9

Detachable Abstract Cards

1. Introduction.

There has been little direct information available on the behaviour of three-dimensional turbulent boundary layers in supersonic flow. The state of knowledge in 1961/62 has been described by Cooke and Hall¹. To make a calculation of such a boundary layer a small cross-flow approximation can be attempted, on the lines followed for three-dimensional laminar boundary layers, and a correlation between compressible and incompressible boundary layers can be sought; but since the boundary layer is turbulent a number of assumptions are needed, and the lack of an experimental basis for the assumptions has meant that the results would be no more than tentative. The present work* is a contribution towards this experimental basis, in which the ultimate aim is an understanding of, and an ability to predict, the behaviour of the boundary layer. A set of experimental results is presented in detail, in a form which, it is hoped, will help efforts at understanding and prediction. Whether the results are consistent with current concepts of three-dimensional boundary-layer structure is discussed, but no attempt is made to develop a method of calculating boundary-layer behaviour.

It has become clear from the earlier experimental work that some care has to be exercised in planning the experiment if the amount of information gained is not to be seriously limited. The measurements should cover a region which is sufficiently extensive, both along the external streamlines and laterally across them, to provide information on the growth of the boundary layer with increasing distance downstream and, in addition, on the lateral variations of the properties of the boundary layer (which affect the growth). The measurements must, of course, include the boundary conditions for the boundary layer in this region, namely, the properties of the external flow and of the boundary-layer flow into the region under consideration.

The boundary layer studied here was set up over the plane side-wall of a specially constructed supersonic nozzle. To reduce heat transfer to negligible amounts the wall was made of wood, although it was supported in a metal frame. The nozzle liners were shaped so that the external flow first accelerated and then decelerated, and the cross-wise pressure gradients were such that the boundary-layer cross-flow was first in one direction and then in the opposite, as happens over wings with swept leading edges. The external Mach number ranged between 1.6 and 2.0, and the maximum deviation of the velocity vector in the boundary layer from the local free-stream direction was 12.2 deg. The stream-wise length of the region considered

*A preliminary account², in which the detailed results were omitted, was presented at an AGARD Specialists' Meeting held in Naples, Italy, 10–14 May, 1965.

was about 36 inches (90 cm), and the width varied from 7 to 9 inches (18 to 23 cm); the boundary-layer thickness varied from 0.21 to 0.75 inch (0.54 to 1.9 cm); this permitted the use of probes of Conrad type made from ordinary 0.5 mm (0.020 inch) diameter hypodermic tubing.

Mean values in time of pitot pressure, flow direction, wall static pressure and surface-pitot pressure were measured. Experience with two-dimensional boundary layers suggests that a knowledge of the fluctuating quantities is not needed for approximate methods of calculating skin friction and displacement thickness except near separation, where certain velocity correlations seem to be needed.

The procedure was as follows. After setting up the apparatus (Section 2), the flow direction outside the boundary layer was measured and the paths of three external streamlines were calculated (Section 3). Then (Section 3) the boundary layer was traversed at intervals of one inch (2.54 cm) along these external streamlines, to obtain measurements of pitot pressure and flow direction. To supplement these measurements, a pressure distribution was obtained from a set of static holes in the wall, and surface-pitot measurements were made. The measurements were processed (Section 4) to give distributions of static pressure, external Mach number, skin friction and a selection of momentum and displacement thicknesses; also obtained were boundary-layer profiles of Mach number, flow direction, velocity (including separate profiles of the streamwise and crosswise components of velocity) and temperature. A high-speed computer was used. The complete set of results is tabulated. A discussion (Section 5) of the results is given, in which comparisons are drawn with existing notions of boundary-layer properties. The properties considered are the shapes of the profiles of the cross-flow and the streamwise flow, the shape of the inner part of the streamwise profile in the context of the law of the wall, and the streamwise component of skin friction. Also discussed are estimates of the relative magnitudes of the terms in the streamwise momentum integral equation.

2. Experimental Apparatus.

The work was carried out in one of the interchangeable working sections of the R.A.E. 9" × 9" continuous-running supersonic wind-tunnel. The nozzle contour is shown in Fig. 1. The side-wall opposite that over which the measurements were made was divided into sections of different lengths, so that the particular section carrying the probe could be placed opposite any required section of the boundary layer to be studied. The probe and its gear for traversing and yawing were mounted eccentrically in a rotatable system, so that the probe could reach any required station.

A sketch of the probe and its operating position is shown in Fig. 3. The probe was traversed normal to the wall by a micrometer screw drive, and was yawed by a worm drive. Readings of distance from wall and angular displacement were made to nominal accuracies of 0.001 inch (0.0025 cm) and 0.1 deg respectively. The central pitot tube was connected to a capsule-type manometer; the outer yaw tubes, which were used only in the null-reading mode, were connected to a strain-gauge pressure transducer. The manometer gave readings accurate to within 0.01 inch (0.25 mm) of mercury; the transducer could be balanced much more accurately (~ 0.01 deg) than the scale of angular displacement could be read (0.1 deg).

Readings of static pressure, at holes distributed over the wooden wall, were also taken with the capsule-type manometer. A selection of the holes was used for surface-pitot readings, using the technique suggested by Hool³ and developed for turbulent boundary layers in supersonic flow by Smith, Gaudet and Winter⁴. The surface pitot tubes each consisted of a rectangular piece of razor blade fixed (by double-sided adhesive tape) to the wall, with its sharp leading edge above the leading edge of a circular static hole and roughly at right angles to the local flow direction (see (5) below, and also Section 5.1). The distance from the sharp edge to the wall was 0.0096 ± 0.0002 inch (0.244 ± 0.005 mm), and the orifice formed had an aspect ratio of 20 and was effectively two-dimensional.

A large number of precautions were taken in an effort to make the results obtained reliable:

(1) Over the months during which the measurements were made the head of the probe was subject to a slight twisting distortion (presumably due to residual stresses) which, unless corrected, would result in one of the outer yaw-tubes being closer to the wall than the other. Periodic checks were made.

(2) Some hysteresis was observed in the null position of the probe: the angular reading differed when the position of balance was approached from opposite directions. To obtain smooth profiles it was necessary to approach from the same direction throughout any particular traverse. The discrepancies found by repeating a traverse with the direction of approach reversed varied with the magnitude of the angular displacement from the free-stream direction, the maximum values being about 10 per cent of the angular displacement; so that the maximum errors may be estimated to be ± 5 per cent of the angular displacement.

(3) Some measure of the interference on the boundary layer by the probe is obtained by observing the static pressure on the wall as the probe is traversed. An earlier probe, with a smaller curved portion, interfered seriously in the region of positive streamwise pressure gradient. No effects were observed on the static pressure upstream of the tip of the probe used.

(4) The displacement effect of the probe was crudely estimated by comparing the profiles of pitot pressure obtained with two geometrically similar probes, one with the head made from 0.5 mm tubes and another with its head made from 2 mm tubes, at a station where the boundary layer was sufficiently thick. If z denotes the distance from the wall to the centre of the probe, d the diameter of the probe, and Δz the distance the effective centre of the probe is displaced from the geometric centre (positive in the direction of increasing distance from the wall), the profiles yielded, by linear extrapolation to zero probe diameter, a smooth variation of $\Delta z/d$ from -0.1 , for $z = \frac{1}{2}d$, to 0, for $z = d$, and then to 0.15 , for $z \geq 2d$. This correction was applied to all the measurements with the probe, including those of flow direction; but, in fact, for the diameter of probe used and the thickness of the boundary layer studied, the displacement effect is found to make little difference to the results.

(5) For the measurements with surface pitot tubes, pressures at several positions were obtained in each run of the wind tunnel; checks were made to ensure that there was no mutual interference. One feature of the technique whose importance was not recognised, until attempts were made to repeat readings, was the need to position the leading edge of the blade very accurately over the leading edge of its associated static pressure hole. It was possible, with the method used for mounting the blades, to have position errors of up to 0.005 inch (0.13 mm), and this was found to be sufficient to produce the discrepancies shown, for example, in Fig. 8. On the other hand, little accuracy was needed in aligning the blade relative to the flow direction, because the sensitivity was such that a yaw of even 5 deg produced only a negligible change in reading.

(6) Sample checks for repeatability were made throughout the course of the experiment. Several of the traverses along each of the external streamlines, A, B and C shown in Fig. 1 were repeated. Only when satisfactory agreement was obtained were the results accepted. The chances of spurious results from gas leaks, probe distortions and faulty measuring equipment were in this way minimized. In this period of several months large sections of the apparatus were dismantled and reassembled.

3. Experimental Procedure.

Since it was intended to make boundary-layer traverses at stations along a selection of external streamlines it was necessary first to determine the paths of the streamlines. To do this, the wall was covered by a hypothetical grid with a one-inch (2.54 cm) square mesh, and a measurement of external flow direction was made over each grid point, with the head of the probe at one inch from the wall. The streamline paths were calculated numerically from the flow directions by a simple predictor-corrector method. The streamline passing through a particular station about mid-way between the upstream and downstream ends of the flow field under study would be selected, and the calculation would proceed in one-inch steps both upstream and downstream. Three streamline paths, roughly 2 inches (5 cm) apart, were computed in this way, and they are shown in Fig. 1. For comparison a photograph of a surface oil-flow pattern is shown in Fig. 2; the more pronounced curvature of the surface streamlines is the result of the cross-wise pressure gradients. The ordinates of the streamlines, and of the nozzle liners, are given in Table 1, using the co-ordinate system shown in Fig. 1.

The boundary-layer traverses were straightforward if tedious. For each station, readings of pitot pressure and flow direction were taken from the wall outwards, and continued till no further changes were observed with increasing distance from the wall. The precise point at which the head of the probe

left the wall was determined by observation of the pitot pressure; while the probe pressed lightly on the wall the pitot pressure remained constant; rapid changes in pitot pressure occurred as soon as the probe left the surface.

Each traversing station was identified by the external streamline on which it lay (A, B or C as shown in Fig. 1), and by the distance x in inches from the throat of the nozzle. The stations were spaced at intervals of one inch along each external streamline; along the streamline B, for example, whose path was plotted from $x = 9$ to $x = 46$, there were 36 stations at which traverses were made—traverses could not be made farther downstream than $x = 44$ because the wind tunnel starting shock-wave would move upstream to the probe.

A static pressure distribution was obtained by measuring the pressure at a large number of static holes in the wooden wall. These readings, together with the surface-pitot readings of pressure, provided data for the calculation of skin friction. The static pressures are given in Table 2.

For all the measurements the temperature and pressure in the wind-tunnel settling chamber were maintained at 30 deg C and the prevailing atmospheric value respectively.

4. The Processing of Observations and Presentation of Results.

The Mach number M of the boundary-layer flow was obtained by use of the isentropic-flow equation

$$\frac{p_0}{p} = \left(1 + \frac{\gamma - 1}{2} M^2\right)^{\gamma/(\gamma - 1)}, \quad (1)$$

and the standard pitot-tube equations

$$\frac{p_0}{p'_0} = \left(\frac{2\gamma}{\gamma+1} M^2 - \frac{\gamma-1}{\gamma+1}\right)^{1/(\gamma+1)} \left(\frac{1 + \frac{\gamma-1}{2} M^2}{\frac{\gamma+1}{2} M^2}\right)^{\gamma/(\gamma-1)}, \quad (2)$$

$$\frac{p}{p'_0} = \frac{\left(\frac{2\gamma}{\gamma+1} M^2 - \frac{\gamma-1}{\gamma+1}\right)^{1/(\gamma-1)}}{\left(\frac{\gamma+1}{2} M^2\right)^{\gamma/(\gamma-1)}}, \quad (3)$$

where p_0 , p'_0 and p are the total, pitot (supersonic) and static pressures, respectively, and γ is the ratio of specific heats, taken to be 1.4. The free-stream total pressure was assumed to be equal to the pressure in the settling chamber. First, from equation (2), the Mach number M_e in the external flow was obtained; equation (1) then gave the static pressure, which was assumed to be constant across the boundary layer. The profile of Mach number was then given by equation (3), for the supersonic part of the boundary layer, and by equation (1), for the subsonic part.

The temperature T in the boundary layer was obtained from the energy equation

$$\frac{T_0}{T} = 1 + \frac{\gamma - 1}{2} M^2 \quad (4)$$

on the assumption that the total temperature T_0 in the boundary layer was equal to the temperature in the settling chamber*, and by making use of the Mach numbers derived. This yielded the distribution of density ρ , from the equation of state

$$\rho = \frac{p}{RT}, \quad (5)$$

*This is permissible for the moderate Mach numbers found here; the total temperature is actually nearly constant except very close to the wall, where it falls sharply to the recovery value.

and the distribution of velocity q , from the definition of Mach number

$$q = M (\gamma R T)^{\frac{1}{2}}. \quad (6)$$

The velocity components u and v in the boundary layer, respectively parallel and at right angles to the local direction of the external streamline, were given by the velocity q and the measured flow direction.

The temperature at the wall T_w was assumed to be equal to the recovery temperature and this in turn was assumed to be given by a recovery factor of 0.89. Thus

$$T_w = T_0 - 0.11 \frac{u_e^2}{2 C_p}, \quad (7)$$

where u_e and C_p are the free-stream velocity and the specific heat at constant pressure, respectively. The viscosity at the wall, μ_w , was assumed to be a function of T_w only, and its value was obtained from standard tables.

The profiles of Mach number M , velocity q/u_e , angular displacement β from local free-stream direction, streamwise velocity u/u_e , cross-wise velocity v/u_e , temperature T/T_0 , and $Z = \int_0^\zeta (\rho/\rho_e) d\zeta$ (where ζ is the distance in inches from the wall), were computed automatically using a Mercury digital computer. The last function Z was computed in anticipation of efforts to correlate the compressible boundary layer with an incompressible one. All the profiles are given in Table 3. A selection of the cross-flow profiles is shown in Fig. 4, and a selection of the profiles of streamwise velocity in Fig. 6.

For each station the displacement thickness

$$\delta_1 = \int_0^\infty \left(1 - \frac{\rho u}{\rho_e u_e}\right) d\zeta, \quad (8a)$$

and the momentum thicknesses

$$\theta_{11} = \int_0^\infty \left(1 - \frac{u}{u_e}\right) \frac{\rho u}{\rho_e u_e} d\zeta \quad (8b)$$

$$\theta_{21} = \int_0^\infty -\frac{\rho uv}{\rho_e u_e^2} d\zeta \quad (8c)$$

$$\theta_{12} = \int_0^\infty \left(1 - \frac{u}{u_e}\right) \frac{\rho v}{\rho_e u_e^2} d\zeta \quad (8d)$$

$$\theta_{22} = \int_0^\infty -\frac{\rho v^2}{\rho_e u_e^2} d\zeta, \quad (8e)$$

which occur in the momentum integral equations in streamline co-ordinates (see for example Ref. 1), were evaluated. Also evaluated were certain 'incompressible' quantities sometimes found useful. These are δ_i and θ_i , given by the formulae (8a) and (8b) above with $\rho/\rho_e \equiv 1$, and the 'shape factor' $H_i = \delta_i/\theta_i$. All are given in Table 4.

The local skin-friction coefficient

$$c_f = \frac{\tau_w}{\frac{1}{2} \rho_e u_e^2}$$

was evaluated from the surface-pitot and wall static-pressure measurements by using the empirical formula for τ_w , the shearing stress at the wall,

$$\frac{\rho_w h^2 \tau_w}{\mu_w} = 0.207 \left(\frac{\rho_w h^2 \Delta p}{\mu_w} \right)^{0.764} \quad (9)$$

proposed by Smith, Gaudet and Winter⁴. The quantity h is the distance of the leading edge of the mounted blade from the wall (here $h = 0.0096 \pm 0.0002$ inch), and Δp is the difference between the surface pitot pressure and the static pressure. The calculated values of the local skin-friction coefficient are given in Table 5. For stations beyond those covered by the surface-pitot measurements, the traversing pitot-tube was regarded as a Preston tube, and the surface shear stress τ_w was deduced from the pitot pressure measured with the tube just touching the surface, using the empirical formula

$$\frac{\rho_w h^2 \tau_w}{\mu_w} = 0.198 \left(\frac{\rho_w h^2 \Delta p}{\mu_w} \right)^{0.721},$$

where h here is the overall height (0.5 mm) of the tube.

This formula was derived by comparing the results of the two methods of measurement in the region of overlap; it is only a rough fit, with a maximum error of ± 6 per cent.

5. Discussion of the Results.

5.1. Profiles of Cross-flow.

In Fig. 4 measured profiles of cross-flow, at stations along the external streamline B, are compared with the 'parabolic' form proposed by Mager⁵, Braun⁶ and Cooke⁷; and in Fig. 5 the profiles are plotted in polar form, to allow a comparison with the flow model of Johnston⁸. We consider these in turn.

The parabolic cross-flow profile of Mager, Braun and Cooke is

$$\frac{v}{u_e} = \left(1 - \frac{\zeta}{\delta} \right)^2 a \frac{u}{u_e}, \quad (10)$$

where

$$a = \lim_{\zeta \rightarrow 0} \left(\frac{v}{u} \right),$$

and δ is the boundary-layer thickness. By definition, therefore, this profile must become increasingly accurate as the wall is approached. The parabolic profiles are plotted here by using the measured values of u/u_e and estimated values of a , obtained by extrapolating the measured flow direction linearly to the wall*. It can be seen from Fig. 4 that only in the upstream part of the boundary layer is the parabolic form satisfactory; farther downstream it is totally inadequate. No improvement is obtained by replacing the physical ordinate ζ/δ in equation (10) by the correlating variable (see for example Spence⁹)

$$Z/Z_\delta = \left(\int_0^{\zeta} \frac{\rho}{\rho_e} d\zeta \right) \left/ \left(\int_0^{\delta} \frac{\rho}{\rho_e} d\zeta \right) \right. . \quad (11)$$

Johnston⁸ suggested, for the cross-flow profile, the composite form

$$\frac{v}{u_e} = a \frac{u}{u_e} \quad (12a)$$

near the wall, and

$$\frac{v}{u_e} = C \left(1 - \frac{u}{u_e} \right) \quad (12b)$$

in the outer part, where C is a constant. It follows from the definition of a that the form (12a) must be correct sufficiently close to the wall. The adequacy of the form (12b) may be checked by making a polar plot of v/u_e against au/u_e ; in Johnston's model the outer part of the polar profile is a straight line. A set of polar profiles is shown in Fig. 5; and it is clear that the downstream profiles, at $x = 37$ and $x = 39$, do not fit Johnston's model.

The formulae (10) and (12) above are the simplest and most commonly used** formulae for cross-flow profiles, and it has been shown that both are inadequate for the downstream part of a flow where the cross-flow is in a direction opposite to what it was upstream. An obvious, but hardly helpful, conclusion is that the real situation is too complicated to be represented by such simple formulae. It means that much more account needs to be taken of the upstream history of the boundary layer, at least when the streamwise pressure gradients are adverse. Simple modifications of (10) have been tried without success; in these the profile was assumed to depend as well on a parameter involving the curvature of the external streamline.

5.2. Streamwise Flow.

Analysis of the streamwise flow has been limited, in this Report, to brief examinations of the overall profiles, the inner parts of the profiles (law of the wall) and the measurements of skin friction. In Fig. 6 are shown measured profiles of the streamwise velocity component at three stations along the streamline B. If the component at the station $x = 28$, where the pressure gradients and cross-flow are negligible, is plotted against Z/Z_δ instead of ζ/δ , the profile is found to be accurately given by

$$\frac{u}{u_e} = \left(\frac{Z}{Z_\delta} \right)^{1/7} . \quad (13)$$

*All the measurements near the wall showed that the flow direction there varied very little along the normal to the wall.

**Perry and Joubert¹⁰ have discussed the limitations of Johnston's model, and find that it is appropriate only for flows past bodies of special geometry.

But the other profiles, at stations where the streamwise pressure gradient is appreciable, do not satisfy this power law; the differences in shape cannot be reduced by plotting the velocity component against Z/Z_δ instead of ζ/δ . However, the differences are in the sense found in two-dimensional boundary layers with streamwise pressure gradients, and this suggests that two-dimensional representations of profiles which incorporate a shape-factor or some measure of the pressure gradient might be usefully adopted. Some evidence for this is found in the inner parts of the measured streamwise profiles, three of which have been plotted in Fig. 7, in the form $u/u_e : \log(\zeta u_e/v_w)$, where $u_e = (\tau_{01}/\rho_w)^{1/2}$ and $v_w = \mu_w/\rho_w$ and where τ_{01} was obtained from the surface-pitot measurements. The three profiles, which are respectively associated with positive, negligible and negative streamwise pressure gradients (but which are otherwise chosen at random), all tend to the same straight line and, moreover, this line is virtually the same as those obtained by Smith, Gaudet and Winter⁴ and by Smith and Walker¹¹ for two-dimensional boundary layers. Further evidence for the quasi-two-dimensional character of the streamwise flow is provided by a comparison of estimated and measured values of skin friction. In Fig. 8 are plotted distributions, along the external streamlines B and C, of the streamwise component of skin friction, estimated from the semi-empirical formula

$$\frac{\tau_{01}}{\frac{1}{2} \rho_e u_e^2} = 0.0176 \frac{\rho_m}{\rho_e} \left(\frac{\rho_e u_e \theta_{11}}{\mu_m} \right)^{-\frac{1}{2}} \quad (14)$$

proposed by Spence¹² for two-dimensional boundary layers at constant pressure, where ρ_m and μ_m are evaluated at the intermediate temperature T_m given by

$$T_m = 0.5(T_e + T_w) + 0.22(T_w - T_e).$$

Measured values are also plotted. There is good agreement except where the pressure gradients are pronounced, and there the differences are in the sense that would be expected of a corresponding two-dimensional boundary layer. Thus a formula incorporating a shape-factor would be expected to improve agreement.

5.3. Momentum Integral Equations.

An attempt has been made to estimate from the measurements the magnitudes, for the boundary layer studied, of the terms of the complete momentum integral equations¹

$$\begin{aligned} & \left[\frac{1}{\rho_e u_e^2} \frac{\partial}{h_1 \partial \xi} (\rho_e u_e^2 \theta_{11}) + \frac{1}{u_e} \frac{\partial u_e}{h_1 \partial \xi} \delta_1 \right] + \left[-K_1 \theta_{11} \right] + \\ & + \left[\frac{1}{\rho_e u_e^2} \frac{\partial}{h_2 \partial \eta} (\rho_e u_e^2 \theta_{12}) + \frac{1}{u_e} \frac{\partial u_e}{h_2 \partial \eta} (\theta_{21} - \theta_{12}) + K_1 \theta_{22} - K_2 (\theta_{21} + \theta_{12}) \right] \\ & = \frac{\tau_{01}}{\rho_e u_e^2}, \end{aligned} \quad (15a)$$

$$\begin{aligned} & \left[\frac{1}{\rho_e u_e^2} \frac{\partial}{h_1 \partial \xi} (\rho_e u_e^2 \theta_{21}) + K_2 (\theta_{11} + \delta_1) - 2K_1 \theta_{21} \right] + \\ & + \left[\frac{1}{\rho_e u_e^2} \frac{\partial}{h_2 \partial \eta} (\rho_e u_e^2 \theta_{22}) - K_2 \theta_{22} \right] \\ & = \frac{\tau_{02}}{\rho_e u_e^2}; \end{aligned} \quad (15b)$$

where ξ, η are orthogonal curvilinear streamline co-ordinates, with an element of length along an external streamline given by $h_1 \delta\xi$ and an element of length along an orthogonal trajectory given by $h_2 \delta\eta$; and where K_1 and K_2 are the orthogonal and streamline curvatures respectively, given by

$$\left. \begin{aligned} K_1 &= -\frac{1}{h_2} \frac{\partial h_2}{h_1 \partial \xi} \\ K_2 &= -\frac{1}{h_1} \frac{\partial h_1}{h_2 \partial \eta} \end{aligned} \right\} \quad (16)$$

Estimated values of K_1 and K_2 , along the streamline B, are given in Table 6. There are two (differing) estimates of K_2 . The values used were those derived from the geometry of the streamlines; it was checked that, for the accuracy attainable here, it was immaterial which estimate was used.

The object was to obtain a measure of the three-dimensionality of the boundary layer and, in particular, to check on the importance of the convergence or divergence of the external streamlines and of the terms usually omitted in the 'small cross-flow' approximation. High accuracy could not be expected, because a great deal of numerical differentiation of the experimental results was involved, and it was necessary to smooth the experimental distributions in advance, but it was hoped that qualitative conclusions might at least be drawn. For the first, streamwise, momentum equation (15a) this proved correct, but for the cross-wise equation (15b) the terms turned out to be so small as to be comparable with the errors, and no conclusions could be drawn. The following discussion is concerned only with the streamwise momentum equation (15a).

The results are shown graphically in Fig. 9. The figure gives, for stations along the streamline B, a comparison of sums of the expressions in square brackets and the estimates of the streamwise component of skin friction $\tau_{01}/(\rho_e u_e^2)$. The first expression in square brackets contains all the terms required for a purely two-dimensional boundary layer; its magnitude is given by the dotted curve. The first two expressions in square brackets contain all the terms required in the small cross-flow approximation, the second expression being the approximation for streamline convergence on divergence; the magnitude of their sum is given by the curve in broken line. Lastly, the sum of all three expressions in square brackets, which contain all the terms required for any three-dimensional boundary layer, is given by the curve in full line. The streamwise component of skin friction $\tau_{01}/(\rho_e u_e^2)$ was deduced from the surface-pitot and Preston-tube measurements on the assumption that the surface shear direction was the same as the limiting flow direction at the surface.

Fig. 9 shows that the 'small cross-flow' approximation is inadequate, for the boundary layer studied, in the downstream part of the flow, even where the cross-flow is so small (see Table 3) that the maximum deviation of the boundary-layer flow from the local free-stream direction is less than 3 deg. The 'small cross-flow' approximation seems adequate for the upstream part, where the cross-flows are just as large, but where the boundary layer is thinner. It can be checked that the term involving the crosswise gradient of θ_{12} , the crosswise momentum thickness, becomes appreciable downstream; it is omitted in the 'small cross-flow' approximation and accounts for virtually all the discrepancy between the 'small cross-flow' and 'three-dimensional' curves. The fair agreement between the 'three-dimensional' curve and the values for skin friction confirms that the exercise as a whole is sufficiently accurate to be meaningful. One conclusion which may be useful is that if anyone tests a method of calculation based on the conventional 'small cross-flow' approximation, by making a comparison with the present experimental results, he should confine his test to the region upstream of say $x = 30$; the method cannot be expected to succeed further downstream.

It should not be inferred that the 'small cross-flow' approximation will invariably suffer from the limitations found here, although of course care is needed in applying the approximation. The large crosswise gradients found here arise from the geometry of the nozzle liners, and there may be much smaller gradients over wings and bodies in flight.

5.4. Concluding Remarks.

The main objective in this Report has been to present a set of experimental results for a three-dimensional turbulent boundary layer in supersonic flow, in a form which may be useful for anyone either developing a method of calculating such boundary layer or checking a newly-developed method. It is hoped that the tables and the explanations in the text provide all that would be needed. A preliminary analysis of the results is given, to provide some guidance, and it appears that, while simple representations of the cross-flow are inadequate under certain conditions, the streamwise flow may show a two-dimensional structure even where the 'small cross-flow' approximation is invalid. The failures of the 'parabolic' profile for the cross-flow and the 'small cross-flow' approximation may be connected: they take place in the same part of the flow.

Further work is needed before a reliable method of calculation can be developed. A satisfactory treatment of the cross-flow is needed, and a thorough check should be made of the idea that the streamwise flow may be quasi-two-dimensional. At present there is, unfortunately, little agreement about purely two-dimensional boundary layers, when these are compressible, so the most profitable approach would be to study three-dimensional boundary layers at low speeds.

The limitations of the present work should not be overlooked. There is zero heat transfer, and the boundary-layer Reynolds number $R_\theta \equiv \rho_e u_e \theta_{11} / \mu_m$ is limited to the range $2500 < R_\theta < 15000$. The external Mach number M_e is limited to the range $1.6 < M_e < 2$. And, unlike the flow over wings and bodies, the free-stream flow here is two-dimensional.

LIST OF SYMBOLS

a	$\lim_{\zeta \rightarrow 0} \left(\frac{v}{u} \right)$
C	Constant
c_f	$\tau_w / (\frac{1}{2} \rho_e u_e^2)$ local skin-friction coefficient
C_p	Specific heat at constant pressure
d	Diameter of pitot tube
h	Height of surface pitot tube
h_1, h_2	Length parameters in orthogonal curvilinear system ξ, η
H_i	'Incompressible' shape factor, below equation (8)
K_1, K_2	Orthogonal and streamline curvatures, equations (16)
M	Mach number
p	Static pressure
p_0	Total pressure
p'_0	Pitot pressure
q	Velocity
R	Gas constant
R_θ	$\rho_e u_e \theta_{11} / \mu_m$, Reynolds number
T	Temperature
T_0	Total temperature
T_r	Recovery temperature
u	Streamwise component of velocity
u_t	$(\tau_{01}/\rho_w)^{\frac{1}{2}}$, friction velocity
v	Crosswise component of velocity
x	Distance from throat of nozzle
Z_δ	$\int_0^\delta (\rho/\rho_e) d\xi$
Z	$\int_0^\zeta (\rho/\rho_e) d\xi$

z	Distance from wall to geometric centre of pitot tube
β	Angular displacement from local free-stream direction
γ	Ratio of specific heats
δ	Boundary-layer thickness
δ_1	Displacement thickness, equation (8)
δ_i	'Incompressible' displacement thickness, below equation (8)
ζ	Distance from wall
η	Co-ordinate in orthogonal curvilinear system ξ, η of streamline co-ordinates
$\theta_{11}, \theta_{21}, \theta_{12}, \theta_{22}$	Various momentum thicknesses, equation (8)
θ_i	'Incompressible' momentum thicknesses, below equation (8)
μ	Viscosity
ν	μ/ρ kinematic viscosity
ξ	Co-ordinate in orthogonal curvilinear system ξ, η of streamline co-ordinates
ρ	Density
τ	Shearing stress
τ_{01}, τ_{02}	Streamwise and crosswise components of shearing stress at wall

Subscripts

e	Denotes conditions in the external flow
m	Denotes conditions at the intermediate temperature, below equation (15)
w	Denotes conditions at the wall

REFERENCES

<i>No.</i>	<i>Author(s)</i>	<i>Title, etc.</i>
1	J. C. Cooke and M. G. Hall	Boundary layer in three dimensions. <i>Progress in Aeronautical Science</i> , 2, p. 221, Pergamon Press, 1962.
2	M. G. Hall .. .	Experimental measurements in a three-dimensional turbulent boundary layer in supersonic flow. Paper in ' <i>Recent Developments in Boundary-Layer Research</i> ', AGARDograph 97, Part II, p. 829, 1965.
3	J. N. Hool .. .	Measurement of skin friction using surface tubes. <i>Aircraft Engineering</i> , 28, pp. 52-54, 1956.
4	K. G. Smith, L. Gaudet and .. . K. G. Winter	The use of surface pitot tubes as skin friction meters at supersonic speeds. A.R.C., R. & M. 3351, June 1962.
5	A. Mager .. .	Generalization of boundary-layer momentum-integral equations to three-dimensional flows including those of a rotating system. NACA Report No. 1067, 1952.
6	W. H. Braun .. .	Turbulent boundary layer on a yawed cone in a supersonic stream. NACA TN 4208, 1959.
7	J. C. Cooke .. .	A calculation method for three-dimensional turbulent boundary layers. A.R.C., R. & M. No. 3199, October 1958.
8	J. P. Johnston .. .	The three-dimensional turbulent boundary layer. M.I.T. Gas Turbine Laboratory Report No. 39, 1957.
9	D. A. Spence .. .	Velocity and enthalpy distributions in the compressible turbulent boundary layer on a flat plate. <i>J. Fluid Mech.</i> , 8, pp. 368-387, 1960.
10	A. E. Perry and P. N. Joubert	A three-dimensional turbulent boundary layer. <i>J. Fluid Mech.</i> , 22, pp. 285-304, 1965.

TABLE 1

Ordinates of External Streamlines and Liners.

Distance from throat <i>x</i> (inches)	Ordinate <i>y</i> (inches)				
	Liner	A	B	C	Liner
8	10.710				3.604
9		8.632	7.037	5.405	
10	10.986	8.810	7.190	5.511	3.589
11		8.976	7.324	5.607	
12	11.331	9.124	7.445	5.688	3.576
13		9.260	7.552	5.751	
14	11.616	9.384	7.645	5.796	3.561
15		9.495	7.719	5.828	
16	11.860	9.593	7.778	5.851	3.548
17		9.678	7.823	5.868	
18	12.054	9.751	7.859	5.880	3.536
19		9.804	7.886	5.892	
20	12.196	9.845	7.905	5.907	3.521
21		9.882	7.919	5.920	
22	12.305	9.915	7.931	5.932	3.510
23		9.941	7.943	5.948	
24	12.383	9.956	7.957	5.963	3.491
25		9.970	7.972	5.979	
26	12.410	9.984	7.987	5.991	3.498
27		10.000	8.000	6.000	
28	12.437	10.016	8.014	6.010	3.537
29		10.030	8.031	6.025	
30	12.449	10.047	8.048	6.048	3.615
31		10.068	8.068	6.080	
32	12.463	10.091	8.095	6.122	3.738
33		10.114	8.126	6.177	
34	12.469	10.139	8.170	6.238	3.898
35		10.166	8.226	6.310	
36	12.471	10.198	8.291	6.395	4.096
37		10.236	8.368	6.493	
38	12.506	10.285	8.458	6.605	4.325
39		10.353	8.558	6.730	
40	12.566	10.433	8.682	6.864	4.450
41		10.522	8.805	6.974	
42	12.682	10.648	8.923	7.044	4.515
43		10.786	9.035	7.092	
44	12.867	10.922	9.138	7.121	4.610

TABLE 2
Static-pressure Distribution over Wall.

(in inches Hg , with free-stream total pressure = 29.78 in Hg)

y in x in \	5	6	7	8	9	10	11	12
8		6.80		7.06				
10		5.77		6.42				
12		5.14		6.01				
14		4.71		5.30		5.99		
16		4.46		4.86		5.56		
18		4.34		4.55		5.08		
20		4.34		4.35		4.73		
22		4.31		4.27		4.51		
24		4.31		4.29		4.36		
26		4.41		4.31		4.37		
28		4.46		4.32		4.36		
30		4.76		4.43		4.35		
31	5.08	4.88	4.67		4.35			
32		5.05		4.57		4.39		
33	5.33	5.22	5.27	5.17	4.95	4.77	4.59	
34		5.33		4.91		4.44		
35	5.69	5.53	5.29	4.81	4.66	4.74	4.58	4.42
36		5.69				4.71		
37	6.05	5.79	5.64	5.49	5.20	4.98	4.63	5.09
38		5.88		5.62		5.22		
39	5.47	5.80	5.86	5.86	5.71	5.79	5.33	4.37
40		5.45		5.95		5.84		
41		5.26	5.57	5.97	6.06	5.94	5.45	5.32
42		5.21		5.81		5.74		
43			5.27	5.50	5.61	5.75	5.84	5.75
44		5.17		5.12		5.76		
45			5.24		5.12		5.81	5.89

A 14		A 17		A 18		A 19																									
ζ	M	q/u_a	β	u/u_a	v/u_a	T/T ₀	Z	ζ	M	q/u_a	β	u/u_a	v/u_a	T/T ₀	Z	ζ	M	q/u_a	β	u/u_a	v/u_a	T/T ₀	Z	ζ	M	q/u_a	β	u/u_a	v/u_a	T/T ₀	Z
0.000	0.000	0.000	-4.60	0.000	0.000	0.890	0.000	0.000	0.000	0.000	-5.80	0.000	0.000	0.890	0.000	0.000	0.000	0.000	0.000	-5.80	0.000	0.000	0.890	0.000	0.000	0.000					
0.008	0.952	0.640	-4.60	0.638	-0.051	0.847	0.006	0.000	0.000	0.000	-5.80	0.633	-0.054	0.840	0.006	0.000	0.000	0.000	0.000	-5.80	0.633	-0.054	0.840	0.006	0.000	0.000					
0.009	0.951	0.645	-4.60	0.642	-0.052	0.844	0.007	0.000	0.000	0.000	-5.80	0.646	-0.055	0.833	0.006	0.000	0.000	0.000	0.000	-5.80	0.646	-0.055	0.833	0.006	0.000	0.000					
0.013	1.021	0.673	-4.50	0.676	-0.053	0.838	0.010	0.000	0.000	0.000	-5.80	0.682	-0.057	0.816	0.012	0.000	0.000	0.000	0.000	-5.80	0.682	-0.057	0.816	0.012	0.000	0.000					
0.016	1.060	0.700	-4.20	0.698	-0.051	0.816	0.012	0.000	0.000	0.000	-5.80	0.740	-0.041	0.790	0.014	0.000	0.000	0.000	0.000	-5.80	0.740	-0.041	0.790	0.014	0.000	0.000					
0.020	1.093	0.718	-4.00	0.716	-0.050	0.807	0.015	0.000	0.000	0.000	-5.80	0.741	-0.040	0.716	0.015	0.000	0.000	0.000	0.000	-5.80	0.741	-0.040	0.716	0.015	0.000	0.000					
0.026	1.136	0.740	-3.70	0.739	-0.048	0.795	0.020	0.000	0.000	0.000	-5.80	0.742	-0.064	0.780	0.019	0.000	0.000	0.000	0.000	-5.80	0.742	-0.064	0.780	0.019	0.000	0.000					
0.032	1.176	0.761	-3.40	0.759	-0.045	0.783	0.024	0.000	0.000	0.000	-5.80	0.761	-0.061	0.769	0.024	0.000	0.000	0.000	0.000	-5.80	0.761	-0.061	0.769	0.024	0.000	0.000					
0.043	1.244	0.795	-2.70	0.794	-0.037	0.764	0.033	0.000	0.000	0.000	-5.80	0.794	-0.057	0.752	0.033	0.000	0.000	0.000	0.000	-5.80	0.794	-0.057	0.752	0.033	0.000	0.000					
0.053	1.298	0.820	-2.20	0.820	-0.031	0.740	0.041	0.000	0.000	0.000	-5.80	0.820	-0.049	0.735	0.041	0.000	0.000	0.000	0.000	-5.80	0.820	-0.049	0.735	0.041	0.000	0.000					
0.063	1.348	0.844	-1.80	0.843	-0.027	0.733	0.050	0.000	0.000	0.000	-5.80	0.837	-0.044	0.794	0.049	0.000	0.000	0.000	0.000	-5.80	0.837	-0.044	0.794	0.049	0.000	0.000					
0.073	1.390	0.863	-1.40	0.863	-0.021	0.731	0.059	0.000	0.000	0.000	-5.80	0.854	-0.039	0.711	0.057	0.000	0.000	0.000	0.000	-5.80	0.854	-0.039	0.711	0.057	0.000	0.000					
0.083	1.431	0.881	-1.10	0.832	-0.017	0.710	0.067	0.000	0.000	0.000	-5.80	0.869	-0.033	0.701	0.066	0.000	0.000	0.000	0.000	-5.80	0.869	-0.033	0.701	0.066	0.000	0.000					
0.093	1.471	0.898	-0.80	0.898	-0.013	0.693	0.070	0.000	0.000	0.000	-5.80	0.894	-0.032	0.682	0.075	0.000	0.000	0.000	0.000	-5.80	0.894	-0.032	0.682	0.075	0.000	0.000					
0.103	1.505	0.912	-0.50	0.912	-0.008	0.683	0.085	0.000	0.000	0.000	-5.80	0.913	-0.025	0.681	0.085	0.000	0.000	0.000	0.000	-5.80	0.913	-0.025	0.681	0.085	0.000	0.000					
0.113	1.539	0.926	-0.40	0.926	-0.006	0.679	0.094	0.000	0.000	0.000	-5.80	0.927	-0.022	0.676	0.094	0.000	0.000	0.000	0.000	-5.80	0.927	-0.022	0.676	0.094	0.000	0.000					
0.133	1.597	0.950	-0.20	0.950	-0.003	0.662	0.113	0.000	0.000	0.000	-5.80	0.932	-0.015	0.656	0.111	0.000	0.000	0.000	0.000	-5.80	0.932	-0.015	0.656	0.111	0.000	0.000					
0.153	1.647	0.969	-0.10	0.969	-0.002	0.648	0.132	0.000	0.000	0.000	-5.80	0.953	-0.010	0.641	0.132	0.000	0.000	0.000	0.000	-5.80	0.953	-0.010	0.641	0.132	0.000	0.000					
0.173	1.686	0.974	0.00	0.974	0.000	0.638	0.152	0.000	0.000	0.000	-5.80	0.974	-0.009	0.637	0.152	0.000	0.000	0.000	0.000	-5.80	0.974	-0.009	0.637	0.152	0.000	0.000					
0.193	1.711	0.993	0.00	0.993	0.000	0.631	0.171	0.000	0.000	0.000	-5.80	0.983	-0.008	0.628	0.171	0.000	0.000	0.000	0.000	-5.80	0.983	-0.008	0.628	0.171	0.000	0.000					
0.213	1.732	0.997	0.00	0.997	0.000	0.628	0.191	0.000	0.000	0.000	-5.80	0.992	-0.007	0.626	0.191	0.000	0.000	0.000	0.000	-5.80	0.992	-0.007	0.626	0.191	0.000	0.000					
0.233	1.727	0.999	0.00	0.999	0.000	0.626	0.211	0.000	0.000	0.000	-5.80	0.997	-0.006	0.607	0.207	0.000	0.000	0.000	0.000	-5.80	0.997	-0.006	0.607	0.207	0.000	0.000					
0.253	1.728	0.999	0.00	0.999	0.000	0.626	0.231	0.000	0.000	0.000	-5.80	0.999	-0.005	0.605	0.227	0.000	0.000	0.000	0.000	-5.80	0.999	-0.005	0.605	0.227	0.000	0.000					
0.273	1.729	0.999	0.00	0.999	0.000	0.626	0.251	0.000	0.000	0.000	-5.80	0.999	-0.004	0.605	0.247	0.000	0.000	0.000	0.000	-5.80	0.999	-0.004	0.605	0.247	0.000	0.000					
0.313	1.730	1.000	0.00	1.000	0.000	0.625	0.291	0.000	0.000	0.000	-5.80	0.999	-0.003	0.604	0.267	0.000	0.000	0.000	0.000	-5.80	0.999	-0.003	0.604	0.267	0.000	0.000					

TABLE 3—continued. A14-A19

A 31								A 33							
ζ	M	q/u_e	β	u/u_e	v/u_e	T/T_0	Z	ζ	M	q/u_e	β	u/u_e	v/u_e	T/T_0	Z
0.000	0.000	0.000	-3.90	0.000	0.000	0.890	0.000	0.000	0.000	0.000	-3.00	0.000	0.000	0.890	0.000
0.008	0.925	0.587	-3.90	0.586	-0.040	0.854	0.005	0.008	0.900	0.578	-3.00	0.577	-0.030	0.860	0.005
0.009	0.928	0.589	-3.90	0.587	-0.040	0.853	0.006	0.009	0.900	0.581	-3.00	0.580	-0.030	0.859	0.006
0.013	0.958	0.605	-3.90	0.603	-0.041	0.845	0.009	0.013	0.946	0.603	-3.00	0.602	-0.033	0.848	0.009
0.016	I.005	0.629	-3.80	0.628	-0.042	0.833	0.011	0.016	0.983	0.622	-3.00	0.621	-0.034	0.838	0.011
0.020	I.041	0.648	-3.70	0.647	-0.042	0.822	0.014	0.020	I.016	0.640	-3.00	0.639	-0.033	0.829	0.014
0.026	I.086	0.671	-3.60	0.670	-0.042	0.809	0.018	0.026	I.056	0.661	-3.00	0.660	-0.035	0.818	0.018
0.032	I.123	0.689	-3.50	0.688	-0.042	0.798	0.022	0.032	I.091	0.678	-3.00	0.677	-0.036	0.808	0.022
0.043	I.184	0.719	-3.30	0.718	-0.041	0.781	0.030	0.043	I.148	0.707	-2.90	0.706	-0.026	0.791	0.030
0.053	I.234	0.742	-3.20	0.741	-0.041	0.767	0.038	0.053	I.194	0.729	-2.80	0.728	-0.036	0.778	0.038
0.073	I.312	0.777	-3.00	0.776	-0.041	0.744	0.053	0.073	I.268	0.763	-2.70	0.763	-0.036	0.757	0.053
0.093	I.378	0.806	-2.80	0.805	-0.039	0.725	0.068	0.093	I.330	0.791	-2.60	0.790	-0.036	0.739	0.068
0.113	I.434	0.829	-2.60	0.828	-0.038	0.708	0.085	0.113	I.384	0.814	-2.40	0.813	-0.034	0.723	0.084
0.133	I.487	0.850	-2.30	0.850	-0.034	0.694	0.101	0.133	I.434	0.835	-2.20	0.835	-0.032	0.709	0.101
0.163	I.560	0.879	-2.00	0.878	-0.031	0.673	0.126	0.163	I.504	0.863	-2.00	0.863	-0.030	0.689	0.126
0.193	I.628	0.904	-1.60	0.904	-0.025	0.654	0.152	0.193	I.570	0.889	-1.70	0.889	-0.026	0.670	0.151
0.223	I.690	0.926	-1.30	0.926	-0.021	0.636	0.179	0.223	I.633	0.912	-1.40	0.912	-0.022	0.652	0.178
0.253	I.747	0.946	-0.90	0.945	-0.015	0.621	0.207	0.253	I.691	0.933	-1.10	0.933	-0.018	0.636	0.205
0.283	I.798	0.962	-0.60	0.962	-0.010	0.607	0.235	0.283	I.749	0.953	-0.80	0.953	-0.013	0.620	0.233
0.313	I.843	0.977	-0.40	0.977	-0.007	0.596	0.264	0.313	I.796	0.969	-0.60	0.969	-0.010	0.608	0.261
0.343	I.877	0.988	-0.20	0.988	-0.003	0.587	0.293	0.343	I.835	0.981	-0.40	0.981	-0.007	0.598	0.290
0.373	I.900	0.995	-0.10	0.995	-0.002	0.581	0.322	0.373	I.864	0.991	-0.10	0.991	-0.002	0.590	0.319
0.403	I.913	0.998	0.00	0.998	0.000	0.577	0.352	0.403	I.883	0.997	0.00	0.997	0.000	0.585	0.349
0.433	I.917	I.000	0.00	I.000	0.000	0.576	0.382	0.433	I.891	0.999	0.00	0.999	0.000	0.583	0.379
0.493	I.918	I.000	0.00	I.000	0.000	0.576	0.442	0.493	I.894	I.000	0.00	I.000	0.000	0.582	0.439

A 31								A 34							
ζ	M	q/u_e	β	u/u_e	v/u_e	T/T_0	Z	ζ	M	q/u_e	β	u/u_e	v/u_e	T/T_0	Z
0.000	0.000	0.000	-4.40	0.000	0.000	0.890	0.000	0.000	0.000	0.000	-2.00	0.000	0.000	0.890	0.000
0.008	0.927	0.588	-4.40	0.586	-0.045	0.853	0.005	0.008	0.902	0.577	-2.00	0.576	-0.020	0.860	0.005
0.009	0.939	0.595	-4.40	0.593	-0.046	0.850	0.006	0.009	0.908	0.580	-2.00	0.580	-0.020	0.859	0.006
0.013	0.990	0.622	-4.30	0.620	-0.047	0.836	0.009	0.013	0.937	0.596	-2.00	0.596	-0.021	0.851	0.009
0.016	I.031	0.643	-4.20	0.641	-0.047	0.825	0.011	0.016	0.978	0.618	-2.00	0.618	-0.022	0.839	0.011
0.020	I.044	0.660	-4.10	0.658	-0.047	0.813	0.014	0.020	I.021	0.635	-2.00	0.635	-0.022	0.830	0.014
0.026	I.106	0.681	-3.90	0.679	-0.046	0.804	0.018	0.026	I.051	0.656	-2.00	0.656	-0.023	0.819	0.018
0.032	I.139	0.697	-3.70	0.696	-0.045	0.794	0.022	0.032	I.084	0.673	-2.00	0.673	-0.023	0.810	0.022
0.043	I.197	0.725	-3.60	0.723	-0.046	0.777	0.030	0.043	I.137	0.699	-2.00	0.699	-0.024	0.795	0.030
0.053	I.245	0.747	-3.40	0.746	-0.044	0.763	0.038	0.053	I.181	0.720	-2.10	0.720	-0.026	0.782	0.037
0.073	I.321	0.781	-3.20	0.780	-0.044	0.741	0.053	0.073	I.253	0.754	-2.00	0.753	-0.023	0.761	0.052
0.093	I.385	0.809	-2.90	0.808	-0.041	0.723	0.069	0.093	I.313	0.781	-2.00	0.780	-0.027	0.744	0.068
0.113	I.444	0.832	-2.70	0.831	-0.039	0.707	0.085	0.113	I.366	0.804	-1.90	0.804	-0.027	0.728	0.084
0.143	I.513	0.861	-2.40	0.860	-0.036	0.686	0.110	0.143	I.415	0.825	-1.80	0.825	-0.026	0.714	0.100
0.173	I.586	0.888	-2.00	0.888	-0.031	0.665	0.135	0.173	I.483	0.852	-1.60	0.852	-0.024	0.695	0.124
0.203	I.652	0.913	-1.60	0.912	-0.025	0.647	0.162	0.193	I.547	0.878	-1.50	0.877	-0.023	0.676	0.150
0.233	I.712	0.934	-1.30	0.933	-0.021	0.630	0.189	0.233	I.608	0.901	-1.30	0.900	-0.019	0.659	0.176
0.263	I.768	0.952	-0.90	0.952	-0.015	0.615	0.216	0.263	I.665	0.921	-1.00	0.921	-0.016	0.643	0.202
0.293	I.818	0.969	-0.50	0.969	-0.008	0.602	0.245	0.293	I.718	0.940	-0.60	0.940	-0.010	0.629	0.230
0.323	I.860	0.982	-0.30	0.982	-0.005	0.591	0.274	0.323	I.767	0.956	-0.40	0.956	-0.007	0.616	0.258
0.353	I.891	0.992	-0.10	0.992	-0.002	0.583	0.303	0.353	I.810	0.970	-0.30	0.970	-0.005	0.604	0.286
0.383	I.909	0.997	0.00	0.997	0.000	0.578	0.333	0.383	I.846	0.982	-0.10	0.982	-0.003	0.595	0.315
0.413	I.917	0.999	0.00	0.999	0.000	0.576	0.363	0.413	I.872	0.990	-0.10	0.990	-0.002	0.588	0.345
0.443	I.918	I.000	0.00	I.000	0.000	0.576	0.393	0.443	I.889	0.995	0.00	0.995	0.000	0.584	0.374
0.553	I.899	I.000	0.00	I.000	0.000	0.581	0.500	0.553	I.904	I.000	0.00	I.000	0.000	0.580	0.494

TABLE 3—continued. A31-A40

A 44

ζ	M	q/u_a	β	u/u_a	v/u_a	T/T_0	Z
0.000	0.000	0.000	6.20	0.000	0.000	0.890	0.000
0.008	0.757	0.525	6.20	0.532	0.057	0.897	0.006
0.009	0.759	0.527	6.20	0.533	0.057	0.897	0.006
0.013	0.776	0.537	6.20	0.534	0.058	0.893	0.009
0.016	0.792	0.553	6.30	0.549	0.061	0.886	0.011
0.020	0.828	0.569	6.30	0.565	0.062	0.879	0.014
0.026	0.860	0.588	6.30	0.585	0.065	0.871	0.018
0.032	0.886	0.603	6.30	0.600	0.066	0.864	0.023
0.053	0.959	0.646	6.20	0.642	0.070	0.845	0.038
0.083	1.028	0.684	5.60	0.681	0.067	0.826	0.061
0.113	1.079	0.712	4.90	0.709	0.061	0.811	0.084
0.153	1.138	0.743	3.90	0.741	0.051	0.794	0.115
0.193	1.196	0.773	3.10	0.771	0.042	0.778	0.147
0.233	1.252	0.800	2.30	0.800	0.033	0.761	0.179
0.273	1.309	0.827	1.50	0.827	0.022	0.745	0.213
0.313	1.366	0.854	1.00	0.854	0.015	0.728	0.247
0.353	1.431	0.878	0.60	0.878	0.009	0.712	0.282
0.393	1.477	0.903	0.30	0.903	0.005	0.696	0.317
0.433	1.529	0.935	0.10	0.935	0.002	0.681	0.354
0.473	1.579	0.945	0.00	0.945	0.000	0.667	0.391
0.513	1.625	0.963	-0.10	0.963	-0.002	0.654	0.429
0.553	1.663	0.978	-0.10	0.978	-0.002	0.644	0.468
0.593	1.692	0.988	-0.10	0.988	-0.002	0.636	0.507
0.633	1.714	0.997	0.20	0.997	0.000	0.630	0.547
0.693	1.722	0.999	0.00	0.999	0.000	0.638	0.606
0.753	1.723	1.000	0.00	1.000	0.000	0.627	0.666

A 45

ζ	M	q/u_a	β	u/u_a	v/u_a	T/T_0	Z
0.000	0.000	0.000	4.00	0.000	0.000	0.890	0.000
0.008	0.765	0.539	4.00	0.528	0.037	0.895	0.006
0.009	0.769	0.531	4.00	0.530	0.037	0.894	0.006
0.013	0.788	0.543	4.00	0.541	0.038	0.890	0.009
0.016	0.817	0.561	4.10	0.559	0.040	0.882	0.011
0.020	0.842	0.576	4.20	0.574	0.042	0.876	0.014
0.026	0.874	0.595	4.40	0.593	0.046	0.867	0.018
0.032	0.900	0.610	4.60	0.608	0.049	0.860	0.023
0.053	0.973	0.652	4.70	0.650	0.053	0.841	0.038
0.083	1.041	0.690	4.50	0.688	0.054	0.822	0.061
0.113	1.093	0.717	4.00	0.715	0.050	0.807	0.084
0.153	1.151	0.748	3.30	0.746	0.043	0.791	0.115
0.193	1.205	0.775	2.50	0.774	0.035	0.775	0.147
0.233	1.259	0.802	1.90	0.801	0.027	0.759	0.180
0.273	1.314	0.837	1.40	0.837	0.020	0.743	0.213
0.313	1.368	0.852	0.80	0.852	0.012	0.728	0.247
0.353	1.431	0.876	0.50	0.876	0.008	0.712	0.282
0.393	1.474	0.899	0.20	0.899	0.003	0.697	0.317
0.433	1.524	0.920	0.00	0.920	0.000	0.683	0.353
0.473	1.573	0.940	-0.20	0.940	-0.003	0.669	0.390
0.513	1.617	0.957	-0.20	0.957	-0.003	0.657	0.428
0.553	1.656	0.972	-0.30	0.972	-0.005	0.646	0.467
0.593	1.688	0.984	-0.30	0.984	-0.005	0.637	0.506
0.633	1.709	0.992	-0.30	0.992	-0.005	0.631	0.545
0.693	1.724	0.997	-0.30	0.997	-0.005	0.627	0.595
0.753	1.728	0.999	-0.20	0.999	-0.003	0.626	0.664
0.813	1.729	0.999	-0.10	0.999	-0.002	0.626	0.724
0.913	1.731	1.000	0.00	1.000	0.000	0.625	0.824

TABLE 3—continued. A44-A45.

C 9

ζ	M	q/u_e	β	u/u_e	v/u_e	T/T_0	Z	ζ	M	q/u_e	β	u/u_e	v/u_e	T/T_0	Z
0.000	0.000	0.000	-0.50	0.000	0.000	0.890	0.000	0.000	0.000	0.000	-3.80	0.000	0.000	0.890	0.000
0.008	1.021	0.691	-0.50	0.691	-0.006	0.827	0.006	0.008	1.024	0.660	-3.80	0.658	-0.044	0.827	0.006
0.009	1.036	0.700	-0.50	0.700	-0.006	0.823	0.007	0.009	1.045	0.671	-3.80	0.669	-0.044	0.821	0.006
0.013	1.112	0.741	-0.50	0.741	-0.006	0.802	0.010	0.013	1.119	0.709	-3.50	0.708	-0.043	0.800	0.009
0.016	1.165	0.769	-0.40	0.769	-0.005	0.786	0.012	0.016	1.169	0.734	-3.30	0.733	-0.042	0.785	0.012
0.020	1.202	0.788	-0.30	0.788	-0.004	0.776	0.016	0.020	1.209	0.754	-3.00	0.753	-0.039	0.774	0.015
0.026	1.261	0.817	-0.10	0.817	-0.001	0.759	0.021	0.026	1.265	0.780	-2.70	0.779	-0.037	0.758	0.019
0.032	1.310	0.841	0.10	0.841	0.001	0.745	0.026	0.032	1.314	0.803	-2.30	0.803	-0.032	0.743	0.024
0.038	1.354	0.862	0.20	0.862	0.003	0.732	0.031	0.038	1.359	0.833	-2.00	0.823	-0.029	0.730	0.029
0.043	1.389	0.878	0.30	0.878	0.005	0.722	0.035	0.043	1.398	0.840	-1.60	0.840	-0.023	0.719	0.033
0.048	1.425	0.894	0.40	0.894	0.006	0.711	0.040	0.053	1.464	0.868	-1.10	0.868	-0.017	0.700	0.042
0.053	1.452	0.906	0.40	0.906	0.006	0.703	0.044	0.063	1.519	0.890	-0.80	0.890	-0.012	0.684	0.050
0.063	1.496	0.925	0.40	0.925	0.006	0.691	0.053	0.073	1.569	0.910	-0.50	0.910	-0.008	0.670	0.059
0.073	1.525	0.941	0.30	0.941	0.005	0.680	0.063	0.083	1.614	0.947	-0.40	0.927	-0.006	0.657	0.068
0.083	1.569	0.955	0.10	0.955	0.002	0.670	0.072	0.093	1.655	0.943	-0.30	0.943	-0.005	0.646	0.078
0.093	1.596	0.966	0.10	0.966	0.002	0.663	0.082	0.103	1.691	0.956	-0.20	0.956	-0.003	0.636	0.087
0.103	1.618	0.975	0.00	0.975	0.000	0.656	0.091	0.113	1.721	0.967	-0.10	0.967	-0.002	0.628	0.097
0.113	1.636	0.982	0.00	0.982	0.000	0.651	0.101	0.133	1.768	0.983	0.00	0.983	0.000	0.615	0.116
0.133	1.661	0.992	0.00	0.992	0.000	0.644	0.120	0.153	1.812	0.998	0.10	0.998	0.002	0.604	0.136
0.153	1.673	0.997	0.00	0.997	0.000	0.641	0.141	0.173	1.817	0.999	0.10	0.999	0.002	0.602	0.155
0.173	1.678	0.999	-0.10	0.999	-0.002	0.640	0.161	0.213	1.819	1.000	0.00	1.000	0.000	0.602	0.195
0.193	1.680	0.999	0.00	0.999	0.000	0.639	0.181	0.213	1.682	1.000	0.00	1.000	0.000	0.602	0.195

C 10

ζ	M	q/u_e	β	u/u_e	v/u_e	T/T_0	Z
0.000	0.000	0.000	-1.90	0.000	0.000	0.890	0.000
0.008	1.020	0.676	-1.90	0.676	-0.022	0.828	0.006
0.009	1.046	0.690	-1.90	0.690	-0.023	0.821	0.007
0.013	1.123	0.731	-1.80	0.731	-0.023	0.799	0.010
0.016	1.173	0.757	-1.60	0.756	-0.021	0.784	0.012
0.020	1.214	0.777	-1.40	0.777	-0.019	0.772	0.015
0.026	1.273	0.806	-1.00	0.806	-0.014	0.755	0.020
0.032	1.321	0.829	-0.80	0.829	-0.012	0.741	0.025
0.038	1.366	0.849	-0.60	0.849	-0.009	0.728	0.030
0.043	1.405	0.867	-0.40	0.867	-0.006	0.717	0.035
0.053	1.469	0.894	-0.10	0.894	-0.002	0.699	0.043
0.063	1.519	0.915	0.10	0.915	0.002	0.684	0.052
0.073	1.563	0.933	0.10	0.933	0.002	0.673	0.062
0.083	1.601	0.948	0.00	0.948	0.000	0.661	0.071
0.093	1.633	0.961	-0.10	0.961	-0.003	0.652	0.080
0.103	1.660	0.971	-0.20	0.971	-0.003	0.645	0.090
0.113	1.681	0.979	-0.20	0.979	-0.003	0.639	0.100
0.133	1.712	0.990	-0.20	0.990	-0.003	0.630	0.119
0.153	1.728	0.996	-0.10	0.996	-0.002	0.626	0.139
0.173	1.736	0.999	0.00	0.999	0.000	0.624	0.159
0.193	1.734	0.998	0.00	0.998	0.000	0.624	0.179
0.213	1.739	1.000	0.00	1.000	0.000	0.623	0.199

C 11

ζ	M	q/u_e	β	u/u_e	v/u_e	T/T_0	Z	ζ	M	q/u_e	β	u/u_e	v/u_e	T/T_0	Z
0.000	0.000	0.000	-2.60	0.000	0.000	0.890	0.000	0.000	0.000	0.000	-5.40	0.000	0.000	0.890	0.000
0.008	1.038	0.669	-2.60	0.668	-0.030	0.825	0.006	0.009	1.024	0.643	-5.40	0.640	-0.060	0.830	0.005
0.009	1.050	0.681	-2.60	0.680	-0.031	0.819	0.006	0.013	1.100	0.688	-5.10	0.686	-0.061	0.825	0.006
0.013	1.129	0.721	-2.50	0.721	-0.031	0.797	0.009	0.016	1.148	0.712	-4.80	0.709	-0.060	0.792	0.011
0.016	1.180	0.747	-2.20	0.746	-0.029	0.782	0.012	0.016	1.186	0.730	-4.50	0.728	-0.057	0.781	0.014
0.020	1.220	0.767	-2.00	0.766	-0.027	0.771	0.015	0.026	1.240	0.756	-4.20	0.754	-0.055	0.765	0.019
0.026	1.278	0.794	-1.60	0.794	-0.022	0.754	0.020	0.032	1.286	0.777	-3.80	0.776	-0.052	0.751	0.024
0.032	1.333	0.820	-1.30	0.820	-0.019	0.738	0.025	0.043	1.364	0.813	-3.00	0.811	-0.042	0.729	0.032
0.038	1.373	0.837	-1.00	0.837	-0.015	0.726	0.030	0.053	1.429	0.839	-2.40	0.839	-0.035	0.710	0.040
0.043	1.414	0.855	-0.80	0.855	-0.012	0.714	0.034	0.063	1.485	0.863	-1.90	0.862	-0.039	0.694	0.049
0.048	1.447	0.869	-0.60	0.869	-0.009	0.705	0.038	0.073	1.537	0.883	-1.50	0.883	-0.023	0.679	0.057
0.053	1.479	0.883	-0.40	0.883	-0.006	0.696	0.042	0.093	1.586	0.902	-1.20	0.902	-0.019	0.665	0.066
0.063	1.513	0.905	-0.30	0.905	-0.005	0.680	0.051	0.103	1.631	0.919	-0.90	0.919	-0.014	0.653	0.075
0.073	1.580	0.923	-0.10	0.923	-0.002	0.667	0.060	0.113	1.672	0.933	-0.60	0.933	-0.010	0.641	0.084
0.083	1.622	0.940	-0.20	0.940	-0.003	0.655	0.070	0.123	1.709	0.947	-0.40	0.947	-0.007	0.631	0.093
0.093	1.658	0.953	-0.20	0.953	-0.003	0.645	0.079	0.133	1.774	0.969	-0.20	0.969	-0.003	0.614	0.112
0.103	1.689	0.965	-0.20	0.965	-0.003	0.637	0.089	0.153	1.820	0.984	0.00	0.984	0.000	0.601	0.132
0.113	1.716	0.974	-0.20	0.974	-0.003	0.629	0.098	0.173	1.849	0.993	0.10	0.993	0.002	0.594	0.151
0.133	1.753	0.987	-0.20	0.987	-0.003	0.619	0.118	0.193	1.862	0.997	0.10	0.997	0.002	0.591	0.171
0.153	1.774	0.995	-0.10	0.995	-0.002	0.614	0.137	0.213	1.866	0.999	0.10	0.999	0.002	0.589	0.191
0.173	1.784	0.998	-0.10	0.998	-0.002	0.611	0.157	0.233	1.868	0.999	0.00	0.999	0.000	0.589	0.211
0.193	1.788	1.000	0.00	1.000	0.000	0.610	0.177	0.253	1.870	1.000	0.00	1.000	0.000	0.589	0.231
0.213	1.789	1.000	0.00	1.000	0.000	0.610	0.197								

TABLE 3—continued. C9-C14.

C 20							
ζ	M	q/u_e	β	u/u_e	v/u_e	T/T_0	Z
0.000	0.000	0.000	-4.40	0.000	0.000	0.890	0.000
0.008	0.951	0.601	-4.40	0.599	-0.046	0.847	0.005
0.009	0.987	0.620	-4.40	0.618	-0.048	0.837	0.006
0.013	1.037	0.646	-4.30	0.644	-0.048	0.823	0.009
0.016	1.076	0.666	-4.20	0.664	-0.049	0.812	0.011
0.020	1.106	0.681	-4.10	0.679	-0.049	0.803	0.014
0.020	I.149	0.702	-4.00	0.700	-0.049	0.791	0.018
0.032	I.187	0.720	-3.00	0.718	-0.049	0.780	0.022
0.043	I.251	0.750	-3.70	0.748	-0.048	0.762	0.031
0.053	I.307	0.775	-3.50	0.774	-0.047	0.745	0.038
0.063	I.357	0.797	-3.20	0.796	-0.044	0.731	0.046
0.073	I.401	0.816	-2.90	0.814	-0.041	0.718	0.054
0.093	I.481	0.848	-2.40	0.847	-0.036	0.695	0.070
0.113	I.555	0.877	-1.90	0.877	-0.029	0.674	0.087
0.133	I.624	0.903	-1.60	0.902	-0.025	0.655	0.105
0.153	I.687	0.925	-1.20	0.925	-0.019	0.637	0.123
0.173	I.748	0.946	-0.80	0.946	-0.013	0.621	0.141
0.193	I.803	0.964	-0.50	0.964	-0.008	0.606	0.160
0.213	I.850	0.979	-0.30	0.979	-0.005	0.594	0.179
0.233	I.886	0.990	-0.10	0.990	-0.002	0.584	0.198
0.253	I.906	0.996	-0.10	0.996	-0.002	0.579	0.218
0.273	I.915	0.999	0.00	0.999	0.000	0.577	0.238
0.293	I.919	I.000	0.00	I.000	0.000	0.576	0.258

C 23							
ζ	M	q/u_e	β	u/u_e	v/u_e	T/T_0	Z
0.000	0.000	0.000	-4.40	0.000	0.000	0.890	0.000
0.008	0.945	0.599	-4.40	0.597	-0.043	0.848	0.005
0.009	0.963	0.608	-4.40	0.607	-0.043	0.844	0.006
0.013	I.020	0.638	-4.00	0.637	-0.045	0.828	0.009
0.016	I.061	0.659	-3.90	0.657	-0.045	0.816	0.011
0.020	I.093	0.675	-3.80	0.674	-0.045	0.807	0.014
0.026	I.137	0.697	-3.70	0.696	-0.045	0.794	0.018
0.032	I.174	0.715	-3.60	0.713	-0.045	0.784	0.022
0.043	I.237	0.744	-3.40	0.743	-0.044	0.766	0.031
0.053	I.291	0.769	-3.20	0.768	-0.043	0.750	0.038
0.063	I.339	0.790	-3.00	0.789	-0.040	0.736	0.046
0.073	I.391	0.808	-2.80	0.807	-0.039	0.724	0.054
0.093	I.458	0.840	-2.40	0.839	-0.035	0.702	0.070
0.113	I.529	0.868	-2.00	0.867	-0.030	0.681	0.087
0.133	I.597	0.894	-1.70	0.893	-0.027	0.662	0.104
0.153	I.660	0.916	-1.30	0.916	-0.021	0.645	0.123
0.173	I.718	0.937	-1.00	0.937	-0.016	0.629	0.140
0.193	I.773	0.955	-0.70	0.955	-0.012	0.614	0.158
0.213	I.821	0.971	-0.40	0.971	-0.007	0.601	0.177
0.233	I.861	0.984	-0.30	0.984	-0.005	0.591	0.197
0.253	I.889	0.992	-0.20	0.992	-0.003	0.584	0.216
0.273	I.904	0.997	-0.10	0.997	-0.002	0.580	0.236
0.293	I.911	0.999	0.00	0.999	0.000	0.578	0.256
0.313	I.914	I.000	0.00	I.000	0.000	0.577	0.276
0.333	I.915	I.000	0.00	I.000	0.000	0.577	0.296

C 21							
ζ	M	q/u_e	β	u/u_e	v/u_e	T/T_0	Z
0.000	0.000	0.000	-4.40	0.000	0.000	0.890	0.000
0.008	0.945	0.599	-4.40	0.597	-0.043	0.844	0.005
0.009	0.963	0.608	-4.40	0.607	-0.043	0.844	0.006
0.013	I.020	0.638	-4.00	0.637	-0.045	0.828	0.009
0.016	I.061	0.659	-3.90	0.657	-0.045	0.816	0.011
0.020	I.093	0.675	-3.80	0.674	-0.045	0.807	0.014
0.026	I.137	0.697	-3.70	0.696	-0.045	0.794	0.018
0.032	I.174	0.715	-3.60	0.713	-0.045	0.784	0.022
0.043	I.237	0.744	-3.40	0.743	-0.044	0.766	0.031
0.053	I.291	0.769	-3.20	0.768	-0.043	0.750	0.038
0.063	I.339	0.790	-3.00	0.789	-0.040	0.736	0.046
0.073	I.391	0.808	-2.80	0.807	-0.039	0.724	0.054
0.093	I.458	0.840	-2.40	0.839	-0.035	0.702	0.070
0.113	I.529	0.868	-2.00	0.867	-0.030	0.681	0.087
0.133	I.597	0.894	-1.70	0.893	-0.027	0.662	0.104
0.153	I.660	0.916	-1.30	0.916	-0.021	0.645	0.123
0.173	I.718	0.937	-1.00	0.937	-0.016	0.629	0.140
0.193	I.773	0.955	-0.70	0.955	-0.012	0.614	0.158
0.213	I.821	0.971	-0.40	0.971	-0.007	0.601	0.177
0.233	I.861	0.984	-0.30	0.984	-0.005	0.591	0.197
0.253	I.889	0.992	-0.20	0.992	-0.003	0.584	0.216
0.273	I.904	0.997	-0.10	0.997	-0.002	0.580	0.236
0.293	I.911	0.999	0.00	0.999	0.000	0.578	0.256
0.313	I.914	I.000	0.00	I.000	0.000	0.577	0.276
0.333	I.915	I.000	0.00	I.000	0.000	0.577	0.296

C 24							
ζ	M	q/u_e	β	u/u_e	v/u_e	T/T_0	Z
0.000	0.000	0.000	-3.70	0.000	0.000	0.890	0.000
0.008	0.947	0.595	-3.70	0.594	-0.038	0.850	0.005
0.009	0.947	0.595	-3.70	0.598	-0.039	0.848	0.006
0.013	I.020	0.628	-3.60	0.627	-0.039	0.833	0.009
0.016	I.045	0.650	-3.50	0.649	-0.040	0.821	0.011
0.020	I.078	0.667	-3.40	0.666	-0.040	0.811	0.014
0.026	I.122	0.689	-3.30	0.687	-0.040	0.799	0.018
0.032	I.159	0.707	-3.20	0.706	-0.039	0.788	0.022
0.043	I.219	0.735	-3.00	0.734	-0.038	0.771	0.030
0.053	I.273	0.760	-2.80	0.759	-0.037	0.755	0.038
0.063	I.301	0.794	-2.60	0.798	-0.035	0.730	0.053
0.073	I.346	0.810	-2.40	0.809	-0.030	0.708	0.069
0.093	I.446	0.858	-1.80	0.857	-0.027	0.688	0.086
0.113	I.506	0.883	-1.60	0.883	-0.025	0.668	0.103
0.133	I.571	0.883	-1.40	0.883	-0.025	0.649	0.123
0.153	I.633	0.906	-1.30	0.906	-0.021	0.632	0.142
0.173	I.692	0.927	-1.00	0.926	-0.016	0.636	0.148
0.193	I.748	0.946	-0.70	0.946	-0.012	0.621	0.157
0.213	I.799	0.963	-0.40	0.963	-0.007	0.607	0.175
0.233	I.844	0.977	-0.20	0.977	-0.003	0.595	0.195
0.253	I.878	0.988	0.00	0.988	0.000	0.586	0.214
0.273	I.901	0.995	0.10	0.995	0.002	0.580	0.234
0.293	I.919	0.998	0.10	0.998	0.002	0.577	0.254
0.313	I.917	I.000	0.00	I.000	0.000	0.576	0.274
0.333	I.919	I.000	0.00	I.000	0.000	0.576	0.294

TABLE 3—continued. C20-C24.

ζ	M	u/u_a	β	u/u_e	v/u_a	T/T_o	Z
0.000	0.000	0.000	-3.10	0.000	0.000	0.890	0.000
0.008	0.919	0.585	-3.10	0.584	-0.032	0.855	0.005
0.009	0.937	0.594	-3.10	0.593	-0.032	0.851	0.006
0.013	0.987	0.621	-3.10	0.620	-0.034	0.827	0.009
0.016	I.030	0.643	-3.00	0.643	-0.034	0.825	0.011
0.020	I.061	0.659	-2.90	0.653	-0.033	0.816	0.014
0.026	I.099	0.678	-2.80	0.678	-0.033	0.805	0.018
0.032	I.133	0.695	-2.70	0.694	-0.033	0.796	0.022
0.043	I.189	0.722	-2.60	0.721	-0.033	0.779	0.030
0.053	I.238	0.745	-2.50	0.744	-0.032	0.765	0.038
0.073	I.318	0.781	-2.20	0.780	-0.030	0.742	0.053
0.093	I.336	0.810	-2.00	0.810	-0.028	0.722	0.069
0.113	I.449	0.836	-1.80	0.836	-0.026	0.704	0.085
0.133	I.508	0.860	-1.60	0.859	-0.024	0.687	0.102
0.153	I.508	0.883	-1.40	0.883	-0.022	0.670	0.119
0.173	I.623	0.903	-1.20	0.903	-0.019	0.655	0.136
0.193	I.675	0.922	-0.90	0.922	-0.014	0.641	0.154
0.213	I.725	0.939	-0.70	0.939	-0.011	0.627	0.172
0.233	I.771	0.955	-0.50	0.955	-0.008	0.614	0.191
0.263	I.833	0.975	-0.30	0.975	-0.005	0.598	0.219
0.293	I.878	0.989	-0.10	0.989	-0.002	0.586	0.248
0.323	I.902	0.996	0.00	0.996	0.000	0.580	0.278
0.353	I.911	0.999	0.00	0.999	0.000	0.578	0.308
0.383	I.914	I.000	0.00	I.000	0.000	0.577	0.338
0.413	I.914	I.000	0.00	I.000	0.000	0.577	0.368

ζ	M	u/u_a	β	u/u_e	v/u_a	T/T_o	Z
0.000	0.000	0.000	-2.60	0.000	0.000	0.890	0.000
0.008	0.903	0.578	-2.60	0.578	-0.026	0.860	0.005
0.013	0.933	0.594	-2.60	0.593	-0.026	0.851	0.006
0.016	0.987	0.621	-2.60	0.620	-0.034	0.827	0.009
0.020	I.031	0.643	-2.40	0.643	-0.034	0.816	0.014
0.026	I.099	0.678	-2.30	0.678	-0.033	0.805	0.018
0.032	I.133	0.695	-2.20	0.694	-0.033	0.796	0.022
0.043	I.189	0.722	-2.00	0.721	-0.033	0.779	0.030
0.053	I.238	0.745	-2.00	0.744	-0.032	0.765	0.038
0.073	I.318	0.781	-2.20	0.780	-0.030	0.742	0.053
0.093	I.336	0.810	-2.40	0.810	-0.028	0.722	0.069
0.113	I.449	0.836	-1.80	0.836	-0.026	0.704	0.085
0.133	I.508	0.860	-1.60	0.859	-0.024	0.687	0.102
0.153	I.508	0.883	-1.40	0.883	-0.022	0.670	0.119
0.173	I.623	0.903	-1.20	0.903	-0.019	0.655	0.136
0.193	I.675	0.922	-0.90	0.922	-0.014	0.641	0.154
0.213	I.725	0.939	-0.70	0.939	-0.011	0.627	0.172
0.233	I.771	0.955	-0.50	0.955	-0.008	0.614	0.191
0.263	I.833	0.975	-0.30	0.975	-0.005	0.598	0.219
0.293	I.878	0.989	-0.10	0.989	-0.002	0.586	0.248
0.323	I.902	0.996	0.00	0.996	0.000	0.580	0.278
0.353	I.911	0.999	0.00	0.999	0.000	0.578	0.308
0.383	I.914	I.000	0.00	I.000	0.000	0.577	0.338
0.413	I.914	I.000	0.00	I.000	0.000	0.577	0.368

ζ	M	u/u_a	β	u/u_e	v/u_a	T/T_o	Z
0.000	0.000	0.000	-1.40	0.000	0.000	0.890	0.000
0.008	0.876	0.566	-1.40	0.566	-0.014	0.867	0.005
0.009	0.891	0.574	-1.40	0.574	-0.014	0.863	0.006
0.013	0.939	0.601	-1.40	0.601	-0.015	0.850	0.009
0.016	0.971	0.618	-1.40	0.618	-0.015	0.841	0.011
0.020	0.999	0.633	-1.40	0.633	-0.015	0.834	0.014
0.026	I.036	0.652	-1.40	0.652	-0.016	0.823	0.018
0.032	I.067	0.668	-1.50	0.668	-0.017	0.815	0.022
0.043	I.122	0.696	-1.50	0.696	-0.018	0.799	0.030
0.053	I.165	0.717	-1.50	0.717	-0.019	0.786	0.037
0.073	I.238	0.752	-1.40	0.751	-0.018	0.765	0.053
0.093	I.302	0.781	-1.40	0.781	-0.019	0.747	0.068
0.113	I.359	0.806	-1.30	0.806	-0.018	0.730	0.084
0.133	I.412	0.829	-1.10	0.829	-0.016	0.715	0.100
0.153	I.464	0.850	-1.10	0.850	-0.016	0.700	0.117
0.173	I.515	0.871	-1.00	0.870	-0.015	0.685	0.134
0.193	I.563	0.889	-0.90	0.889	-0.014	0.672	0.151
0.213	I.609	0.906	-0.70	0.906	-0.011	0.659	0.168
0.243	I.675	0.931	-0.50	0.931	-0.008	0.641	0.195
0.273	I.736	0.952	-0.30	0.952	-0.005	0.624	0.223
0.303	I.790	0.970	-0.10	0.970	-0.002	0.609	0.252
0.333	I.835	0.985	0.00	0.985	0.000	0.598	0.281
0.363	I.863	0.994	0.00	0.994	0.000	0.590	0.310
0.393	I.877	0.998	0.00	0.998	0.000	0.587	0.340
0.423	I.883	I.000	0.00	I.000	0.000	0.585	0.370
0.453	I.884	I.000	0.00	I.000	0.000	0.585	0.400

ζ	M	u/u_a	β	u/u_e	v/u_a	T/T_o	Z
0.000	0.000	0.000	0.30	0.000	0.000	0.890	0.000
0.008	0.847	0.556	0.30	0.556	0.003	0.875	0.005
0.009	0.857	0.561	0.30	0.561	0.003	0.872	0.006
0.013	0.901	0.586	0.30	0.586	0.003	0.860	0.009
0.016	0.929	0.602	0.30	0.602	0.003	0.853	0.011
0.020	0.956	0.617	0.20	0.617	0.002	0.845	0.014
0.026	I.092	0.636	0.10	0.636	0.001	0.836	0.018
0.032	I.122	0.652	0.00	0.652	0.000	0.827	0.022
0.043	I.173	0.679	-0.30	0.679	-0.004	0.813	0.030
0.053	I.214	0.699	-0.40	0.699	-0.005	0.801	0.038
0.073	I.284	0.734	-0.60	0.734	-0.008	0.781	0.053
0.093	I.347	0.764	-0.60	0.764	-0.008	0.763	0.068
0.113	I.394	0.790	-0.70	0.790	-0.010	0.746	0.084
0.133	I.456	0.813	-0.70	0.813	-0.010	0.731	0.100
0.153	I.406	0.835	-0.60	0.835	-0.009	0.717	0.116
0.173	I.455	0.856	-0.60	0.855	-0.009	0.703	0.133
0.193	I.525	0.884	-0.60	0.884	-0.009	0.682	0.159
0.213	I.573	0.910	-0.60	0.910	-0.006	0.663	0.185
0.243	I.623	0.934	-0.30	0.934	-0.005	0.646	0.212
0.273	I.673	0.954	-0.10	0.955	-0.002	0.629	0.240
0.303	I.723	0.972	0.00	0.972	0.000	0.616	0.269
0.333	I.876	0.992	0.00	0.992	0.000	0.585	0.307
0.363	I.894	0.998	0.00	0.998	0.000	0.582	0.328
0.393	I.900	I.000	0.00	I.000	0.000	0.594	0.348
0.423	I.902	I.000	0.00	I.000	0.000	0.594	0.370

TABLE 3—continued. C25-C30.

ζ	C	31	M	u/u_e	β	w/u_e	v/u_e	T/T_e	Z	ζ	C	33	M	u/u_e	β	w/u_e	v/u_e	T/T_e	Z
0.000	0.000	0.000	1.20	0.000	0.000	0.000	0.000	0.890	0.000	0.000	0.000	0.000	0.000	4.60	0.000	0.000	0.000	0.890	0.000
0.008	0.837	0.552	1.20	0.552	0.012	0.877	0.005	0.008	0.005	0.008	0.777	0.527	4.60	0.526	0.042	0.892	0.005	0.892	0.005
0.009	0.844	0.556	1.20	0.556	0.012	0.875	0.006	0.008	0.006	0.009	0.793	0.537	4.60	0.535	0.043	0.888	0.006	0.888	0.006
0.013	0.850	0.577	1.20	0.577	0.012	0.866	0.009	0.006	0.009	0.013	0.838	0.564	4.30	0.562	0.042	0.877	0.009	0.877	0.009
0.016	0.869	0.593	1.10	0.593	0.011	0.858	0.011	0.006	0.011	0.016	0.866	0.580	4.20	0.579	0.043	0.869	0.011	0.869	0.011
0.020	0.834	0.607	1.00	0.607	0.011	0.851	0.014	0.006	0.014	0.020	0.889	0.593	4.10	0.592	0.042	0.864	0.014	0.864	0.014
0.026	0.972	0.628	0.90	0.628	0.010	0.841	0.018	0.006	0.018	0.026	0.919	0.611	3.90	0.609	0.042	0.855	0.018	0.855	0.018
0.032	1.002	0.644	0.70	0.644	0.008	0.833	0.022	0.006	0.022	0.032	0.944	0.625	3.70	0.624	0.040	0.849	0.022	0.849	0.022
0.043	1.051	0.670	0.50	0.670	0.006	0.819	0.030	0.006	0.030	0.043	0.988	0.649	3.40	0.648	0.038	0.837	0.030	0.837	0.030
0.053	1.090	0.690	0.30	0.690	0.004	0.808	0.038	0.006	0.038	0.053	1.023	0.668	3.10	0.667	0.036	0.827	0.038	0.827	0.038
0.073	1.158	0.724	0.00	0.724	0.000	0.789	0.052	0.006	0.052	0.073	1.082	0.700	2.50	0.699	0.031	0.810	0.053	0.810	0.053
0.093	1.219	0.754	-0.20	0.754	-0.003	0.771	0.068	0.006	0.068	0.103	1.159	0.739	1.70	0.739	0.022	0.788	0.076	0.788	0.076
0.113	1.274	0.780	-0.30	0.780	-0.004	0.755	0.083	0.006	0.083	0.133	1.229	0.774	1.20	0.773	0.016	0.768	0.099	0.768	0.099
0.133	1.325	0.803	-0.40	0.803	-0.006	0.740	0.099	0.006	0.099	0.163	1.295	0.805	0.80	0.805	0.011	0.749	0.124	0.749	0.124
0.153	1.374	0.825	-0.50	0.825	-0.007	0.726	0.116	0.006	0.116	0.193	1.360	0.835	0.50	0.835	0.007	0.730	0.148	0.730	0.148
0.173	1.421	0.845	-0.50	0.845	-0.007	0.712	0.132	0.006	0.132	0.223	1.423	0.862	0.10	0.862	0.002	0.712	0.174	0.712	0.174
0.203	1.491	0.874	-0.60	0.874	-0.009	0.693	0.158	0.006	0.158	0.253	1.484	0.888	0.00	0.888	0.000	0.694	0.200	0.694	0.200
0.233	1.556	0.900	-0.50	0.900	-0.008	0.674	0.184	0.006	0.184	0.283	1.542	0.912	-0.10	0.912	-0.002	0.678	0.227	0.678	0.227
0.263	1.618	0.924	-0.50	0.924	-0.008	0.656	0.211	0.006	0.211	0.313	1.598	0.934	-0.10	0.934	-0.002	0.662	0.254	0.662	0.254
0.293	1.677	0.945	-0.30	0.945	-0.005	0.640	0.239	0.006	0.239	0.343	1.651	0.954	-0.10	0.954	-0.002	0.647	0.282	0.647	0.282
0.323	1.729	0.964	-0.10	0.964	-0.002	0.626	0.267	0.006	0.267	0.373	1.696	0.971	-0.10	0.971	-0.002	0.635	0.311	0.635	0.311
0.353	1.774	0.979	-0.10	0.979	-0.002	0.614	0.296	0.006	0.296	0.403	1.735	0.985	-0.10	0.985	-0.002	0.624	0.340	0.624	0.340
0.383	1.806	0.990	-0.10	0.990	-0.002	0.605	0.325	0.006	0.325	0.433	1.759	0.993	0.00	0.993	0.000	0.618	0.370	0.618	0.370
0.413	1.825	0.996	-0.10	0.996	-0.002	0.600	0.355	0.006	0.355	0.463	1.772	0.998	0.00	0.998	0.000	0.614	0.400	0.614	0.400
0.443	1.834	0.999	0.00	0.999	0.000	0.598	0.385	0.006	0.385	0.493	1.770	1.000	0.00	1.000	0.000	0.613	0.430	0.613	0.430
0.473	1.837	1.000	0.00	1.000	0.000	0.597	0.415	0.006	0.415	0.523	1.779	1.000	0.00	1.000	0.000	0.612	0.460	0.612	0.460
ζ	C	31	M	u/u_e	β	w/u_e	v/u_e	T/T_e	Z	ζ	C	34	M	u/u_e	β	w/u_e	v/u_e	T/T_e	Z
0.000	0.000	0.000	1.10	0.000	0.000	0.000	0.000	0.890	0.000	0.000	0.000	0.000	0.000	6.20	0.000	0.000	0.000	0.890	0.000
0.008	0.832	0.549	1.10	0.548	0.011	0.878	0.005	0.008	0.005	0.008	0.771	0.524	6.20	0.521	0.057	0.894	0.005	0.894	0.005
0.009	0.844	0.556	1.10	0.556	0.011	0.875	0.006	0.008	0.006	0.009	0.784	0.531	6.20	0.528	0.057	0.891	0.006	0.891	0.006
0.013	0.883	0.578	1.10	0.578	0.011	0.865	0.009	0.006	0.009	0.013	0.817	0.551	6.10	0.548	0.059	0.882	0.009	0.882	0.009
0.016	0.916	0.597	1.00	0.596	0.010	0.856	0.011	0.006	0.011	0.016	0.846	0.568	5.90	0.565	0.058	0.875	0.011	0.875	0.011
0.020	0.943	0.612	1.00	0.611	0.011	0.849	0.014	0.006	0.014	0.020	0.871	0.583	5.80	0.580	0.059	0.868	0.014	0.868	0.014
0.026	0.979	0.631	0.80	0.631	0.009	0.839	0.018	0.006	0.018	0.026	0.903	0.602	5.60	0.599	0.059	0.860	0.018	0.860	0.018
0.032	1.006	0.646	0.70	0.646	0.008	0.832	0.022	0.006	0.022	0.032	0.930	0.617	5.30	0.614	0.057	0.853	0.022	0.853	0.022
0.043	1.055	0.671	0.50	0.671	0.006	0.818	0.030	0.006	0.030	0.043	0.971	0.640	4.90	0.638	0.055	0.841	0.030	0.841	0.030
0.053	1.095	0.692	0.30	0.692	0.004	0.807	0.038	0.006	0.038	0.073	1.065	0.691	3.80	0.689	0.046	0.815	0.053	0.815	0.053
0.073	1.162	0.726	0.00	0.726	0.000	0.787	0.052	0.006	0.052	0.103	1.138	0.729	2.90	0.728	0.037	0.794	0.075	0.794	0.075
0.093	1.220	0.754	-0.10	0.754	-0.001	0.771	0.068	0.006	0.068	0.133	1.207	0.763	2.10	0.763	0.028	0.774	0.099	0.774	0.099
0.113	1.274	0.779	-0.20	0.779	-0.004	0.755	0.083	0.006	0.083	0.163	1.271	0.794	1.50	0.793	0.021	0.756	0.123	0.756	0.123
0.133	1.327	0.803	-0.40	0.803	-0.006	0.740	0.099	0.006	0.099	0.193	1.334	0.823	1.10	0.823	0.016	0.738	0.147	0.738	0.147
0.153	1.376	0.825	-0.50	0.825	-0.007	0.725	0.116	0.006	0.116	0.223	1.397	0.851	0.70	0.851	0.010	0.719	0.173	0.719	0.173
0.173	1.423	0.845	-0.50	0.845	-0.007	0.712	0.132	0.006	0.132	0.253	1.455	0.876	0.50	0.876	0.008	0.702	0.199	0.702	0.199
0.203	1.492	0.874	-0.60	0.873	-0.009	0.692	0.158	0.006	0.158	0.283	1.514	0.901	0.20	0.901	0.003	0.686	0.225	0.686	0.225
0.233	1.558	0.900	-0.50	0.900	-0.008	0.673	0.184	0.006	0.184	0.313	1.569	0.923	0.10	0.923	0.002	0.670	0.252	0.670	0.252
0.263	1.621	0.923	-0.50	0.923	-0.008	0.656	0.211	0.006	0.211	0.343	1.623	0.943	0.10	0.943	0.002	0.655	0.280	0.655	0.280
0.293	1.680	0.945	-0.30	0.945	-0.005	0.639	0.238	0.006	0.238	0.373	1.670	0.961	0.00	0.961	0.000	0.642	0.308	0.642	0.308
0.323	1.733	0.964	-0.20	0.964	-0.003	0.625	0.267	0.006	0.267	0.403	1.712	0.977	0.00	0.977	0.000	0.630	0.337	0.630	0.337
0.353	1.777	0.979	-0.10	0.979	-0.003	0.613	0.296	0.006	0.296	0.433	1.744	0.988	-0.10	0.988	-0.002	0.622	0.366	0.622	0.366
0.383	1.809	0.990	-0.10	0.990	-0.002	0.604	0.325	0.006	0.325	0.463	1.762	0.994	-0.10	0.994	-0.002	0.617	0.396	0.617	0.396
0.413	1.827	0.996	0.00	0.996	0.000	0.600	0.355	0.006	0.355	0.493	1.772	0.998	-0.10	0.998	-0.002	0.614	0.426	0.614	0.426
0.443	1.836	0.999	0.00	0.999	0.000	0.597	0.385	0.006	0.385	0.523	1.776	0.999	-0.10	0.999	-0.002	0.613	0.456	0.613	0.456
0.473	1.839	0.999	0.00	0.999	0.000	0.597	0.415	0.006	0.415	0.553	1.778	1.000	0.00	1.000	0.000	0.613	0.486	0.613	0.486
0.503	1.840	1.000	0.00	1.000	0.000	0.596	0.445	0.006	0.445	0.583	1.788	1.000	0.00	1.000	0.000	0.613	0.516	0.613	0.516
ζ	C	32	M	u/u_e	β	w/u_e	v/u_e	T/T_e	Z	ζ	C	35	M	u/u_e	β	w/u_e	v/u_e	T/T_e	Z
0.000	0.000	0.000	3.00	0.000	0.000	0.000	0.000	0.890	0.000	0.000	0.000	0.000	7.10	0.000	0.000	0.			

ζ	C	36	M	q/u_a	β	u/u_a	v/u_a	T/T_o	Z
0.000	0.000	0.000	9.50	0.000	0.000	0.890	0.000		
0.008	0.757	0.520	9.50	0.513	0.086	0.897	0.006		
0.009	0.770	0.528	9.50	0.521	0.087	0.894	0.006		
0.013	0.798	0.545	9.30	0.538	0.088	0.887	0.009		
0.016	0.824	0.561	9.20	0.554	0.090	0.880	0.011		
0.020	0.846	0.574	9.00	0.567	0.090	0.875	0.014		
0.026	0.877	0.592	8.70	0.585	0.090	0.867	0.018		
0.032	0.900	0.606	8.40	0.599	0.088	0.860	0.023		
0.043	0.940	0.628	8.00	0.623	0.087	0.850	0.030		
0.073	1.023	0.674	6.80	0.670	0.080	0.827	0.053		
0.103	1.088	0.709	5.60	0.706	0.069	0.809	0.075		
0.133	I.149	0.741	4.60	0.739	0.059	0.791	0.099		
0.163	I.207	0.770	3.60	0.769	0.048	0.774	0.122		
0.193	I.263	0.797	2.90	0.766	0.040	0.758	0.147		
0.223	I.320	0.824	2.20	0.824	0.032	0.741	0.171		
0.253	I.377	0.850	1.70	0.850	0.025	0.725	0.197		
0.283	I.431	0.874	I.30	0.874	0.020	0.709	0.223		
0.313	I.486	0.897	0.90	0.897	0.014	0.694	0.249		
0.343	I.538	0.919	0.60	0.919	0.010	0.679	0.276		
0.373	I.587	0.939	0.40	0.938	0.007	0.665	0.304		
0.403	I.635	0.957	0.20	0.957	0.003	0.652	0.332		
0.433	I.676	0.973	0.10	0.972	0.003	0.640	0.361		
0.463	I.710	0.985	0.00	0.985	0.000	0.631	0.390		
0.493	I.732	0.993	0.00	0.993	0.000	0.625	0.420		
0.533	I.748	0.998	0.00	0.998	0.000	0.621	0.460		
0.573	I.752	1.000	0.00	I.000	0.000	0.620	0.500		
0.613	I.753	I.000	0.00	I.000	0.000	0.620	0.540		
ζ	C	36	M	q/u_a	β	u/u_a	v/u_a	T/T_o	Z
0.000	0.000	0.000	9.80	0.000	0.000	0.890	0.000		
0.008	0.766	0.524	9.80	0.516	0.089	0.895	0.006		
0.009	0.774	0.529	9.80	0.522	0.090	0.893	0.006		
0.014	0.818	0.556	9.50	0.548	0.092	0.884	0.010		
0.020	0.851	0.575	9.20	0.568	0.092	0.873	0.014		
0.026	0.879	0.592	9.00	0.585	0.093	0.866	0.018		
0.032	0.903	0.606	8.80	0.599	0.093	0.860	0.022		
0.043	0.945	0.630	8.30	0.623	0.091	0.849	0.030		
0.073	I.027	0.676	7.10	0.670	0.083	0.826	0.053		
0.103	I.091	0.709	6.00	0.706	0.074	0.808	0.075		
0.133	I.150	0.740	4.90	0.737	0.063	0.791	0.099		
0.163	I.200	0.769	3.90	0.768	0.052	0.774	0.122		
0.193	I.265	0.797	3.10	0.796	0.043	0.757	0.146		
0.223	I.319	0.823	2.40	0.821	0.034	0.742	0.171		
0.253	I.373	0.847	1.80	0.846	0.027	0.726	0.196		
0.283	I.428	0.871	I.30	0.871	0.020	0.710	0.222		
0.313	I.482	0.894	I.00	0.894	0.016	0.695	0.249		
0.343	I.534	0.915	0.70	0.915	0.011	0.680	0.276		
0.373	I.584	0.935	0.40	0.935	0.007	0.666	0.303		
0.403	I.630	0.953	0.30	0.953	0.005	0.653	0.331		
0.433	I.672	0.969	0.10	0.969	0.003	0.641	0.360		
0.463	I.707	0.982	0.00	0.982	0.000	0.632	0.389		
0.493	I.732	0.991	0.00	0.991	0.000	0.625	0.419		
0.533	I.750	0.997	0.00	0.997	0.000	0.620	0.458		
0.573	I.756	0.999	0.00	0.999	0.000	0.619	0.498		
0.613	I.758	1.000	0.00	I.000	0.000	0.618	0.538		
ζ	C	37	M	q/u_a	β	u/u_a	v/u_a	T/T_o	Z
0.000	0.000	0.000	I.0.70	0.000	0.000	0.890	0.000		
0.008	0.750	0.518	I.0.70	0.509	0.096	0.899	0.006		
0.009	0.757	0.523	I.0.70	0.514	0.097	0.897	0.006		
0.014	0.791	0.544	I.0.40	0.535	0.098	0.889	0.010		
0.020	0.830	0.567	I.0.20	0.558	0.100	0.879	0.014		
0.026	0.859	0.585	I.0.00	0.576	0.102	0.871	0.018		
0.032	0.882	0.599	9.80	0.590	0.102	0.865	0.023		
0.043	0.920	0.620	9.40	0.612	0.101	0.855	0.031		
0.073	I.003	0.667	8.00	0.660	0.093	0.833	0.053		
0.103	I.063	0.700	6.80	0.695	0.083	0.816	0.075		
0.133	I.117	0.729	5.70	0.725	0.072	0.800	0.099		
0.163	I.170	0.756	4.80	0.753	0.063	0.785	0.122		
0.193	I.223	0.783	3.90	0.781	0.053	0.770	0.146		
0.223	I.277	0.809	3.00	0.808	0.042	0.754	0.171		
0.253	I.330	0.834	2.20	0.833	0.032	0.739	0.196		
0.283	I.381	0.857	I.70	0.856	0.025	0.724	0.222		
0.313	I.433	0.880	I.20	0.880	0.018	0.709	0.248		
0.343	I.483	0.901	0.80	0.901	0.013	0.695	0.274		
0.373	I.533	0.922	0.60	0.922	0.010	0.680	0.302		
0.403	I.581	0.942	0.30	0.942	0.005	0.667	0.329		
0.433	I.625	0.959	0.10	0.959	0.002	0.654	0.358		
0.463	I.664	0.973	0.00	0.973	0.000	0.644	0.387		
0.493	I.694	0.985	-0.10	0.985	-0.002	0.635	0.416		
0.533	I.720	0.994	-0.10	0.994	-0.002	0.628	0.455		
0.573	I.731	0.998	-0.10	0.998	-0.002	0.625	0.495		
0.613	I.735	1.000	0.00	I.000	0.000	0.624	0.535		
0.653	I.736	I.000	0.00	I.000	0.000	0.624	0.575		
ζ	C	38	M	q/u_a	β	u/u_a	v/u_a	T/T_o	Z
0.000	0.000	0.000	I.2.20	0.000	0.000	0.890	0.000		
0.008	0.747	0.518	I.2.20	0.506	0.099	0.890	0.006		
0.009	0.757	0.524	I.2.20	0.512	0.099	0.897	0.006		
0.014	0.796	0.548	I.2.10	0.536	0.105	0.888	0.010		
0.020	0.832	0.570	I.2.00	0.558	0.107	0.877	0.014		
0.026	0.859	0.587	I.1.60	0.587	0.105	0.875	0.018		
0.032	0.881	0.599	I.1.30	0.588	0.117	0.866	0.023		
0.053	0.947	0.618	I.1.20	0.627	0.115	0.848	0.038		
0.073	0.994	0.664	I.1.00	0.655	0.106	0.835	0.053		
0.093	I.103	0.686	I.1.00	0.678	0.103	0.824	0.068		
0.133	I.103	0.723	I.1.00	0.718	0.108	0.818	0.099		
0.173	I.170	0.758	5.60	0.755	0.074	0.785	0.130		
0.213	I.237	0.791	4.40	0.789	0.061	0.766	0.163		
0.253	I.303	0.823	3.30	0.823	0.050	0.742	0.196		
0.293	I.370	0.854	2.40	0.854	0.036	0.727	0.220		
0.333	I.436	0.884	1.60	0.884	0.025	0.712	0.249		
0.373	I.493	0.911	I.10	0.911	0.017	0.694	0.300		
0.413	I.553	0.949	0.60	0.949	0.010	0.677	0.336		
0.453	I.613	0.979	0.40	0.979	0.008	0.661	0.374		
0.493	I.677	0.972	0.20	0.972	0.005	0.651	0.413		
0.533	I.714	0.985	-0.20	0.985	-0.003	0.630	0.452		
0.573	I.739	0.994	-0.20	0.994	-0.003	0.623	0.491		
0.613	I.749	0.998	-0.10	0.998	-0.002	0.620	0.531		
0.653	I.754	1.000	0.00	I.000	0.000	0.619	0.571		
0.693	I.755	I.000	0.00	I.000	0.000	0.619	0.611		

TABLE 3—continued. C36-C40.

C 40

ζ	M	q/u_e	β	u/u_e	v/u_e	T/T_0	Z
0.000	0.000	0.000	6.50	0.000	0.000	0.890	0.000
0.008	0.795	0.542	6.50	0.538	0.061	0.888	0.006
0.009	0.803	0.547	6.50	0.543	0.062	0.886	0.006
0.014	0.839	0.568	6.80	0.564	0.067	0.877	0.010
0.020	0.880	0.593	6.90	0.588	0.071	0.866	0.014
0.026	0.909	0.609	6.90	0.604	0.073	0.858	0.018
0.032	0.932	0.621	7.00	0.617	0.076	0.852	0.023
0.053	0.997	0.659	6.90	0.654	0.079	0.834	0.038
0.093	1.051	0.704	6.20	0.700	0.076	0.811	0.068
0.133	1.146	0.737	5.30	0.734	0.068	0.792	0.099
0.173	1.207	0.768	4.30	0.766	0.058	0.774	0.130
0.213	1.267	0.797	3.30	0.796	0.046	0.757	0.163
0.293	1.390	0.854	1.70	0.853	0.025	0.721	0.236
0.373	1.513	0.906	0.80	0.906	0.013	0.686	0.300
0.453	1.629	0.952	0.20	0.952	0.003	0.653	0.374
0.533	1.717	0.985	-0.10	0.985	-0.002	0.639	0.451
0.613	1.756	0.999	-0.10	0.999	-0.002	0.619	0.530
0.693	1.760	1.000	0.00	1.000	0.000	0.610	0.610

C 41

ζ	M	q/u_e	β	u/u_e	v/u_e	T/T_0	Z
0.000	0.000	0.000	3.90	0.000	0.000	0.890	0.000
0.008	0.807	0.552	3.90	0.551	0.038	0.885	0.006
0.009	0.810	0.553	3.90	0.552	0.038	0.884	0.006
0.013	0.823	0.561	3.90	0.560	0.038	0.881	0.009
0.016	0.834	0.580	3.90	0.578	0.039	0.873	0.011
0.020	0.880	0.595	4.00	0.594	0.042	0.866	0.014
0.026	0.914	0.615	4.20	0.613	0.045	0.857	0.018
0.032	0.942	0.631	4.40	0.629	0.048	0.849	0.023
0.053	1.015	0.671	4.70	0.669	0.055	0.839	0.038
0.083	1.083	0.708	4.80	0.706	0.059	0.810	0.061
0.113	1.136	0.736	4.40	0.734	0.056	0.795	0.084
0.153	1.197	0.767	3.90	0.765	0.052	0.777	0.116
0.193	1.256	0.796	3.20	0.795	0.044	0.760	0.148
0.233	1.316	0.824	2.50	0.823	0.036	0.743	0.181
0.273	1.376	0.852	1.90	0.851	0.028	0.725	0.215
0.313	1.436	0.878	1.40	0.878	0.021	0.708	0.250
0.353	1.493	0.902	1.00	0.903	0.016	0.692	0.285
0.393	1.550	0.926	0.60	0.926	0.010	0.676	0.322
0.423	1.590	0.942	0.40	0.942	0.007	0.664	0.350
0.453	1.628	0.957	0.20	0.957	0.003	0.654	0.378
0.483	1.663	0.970	0.10	0.970	0.002	0.644	0.407
0.513	1.693	0.981	0.10	0.981	0.002	0.636	0.436
0.553	1.720	0.991	0.00	0.991	0.000	0.628	0.475
0.613	1.741	0.998	0.00	0.998	0.000	0.623	0.535
0.673	1.746	1.000	0.00	1.000	0.000	0.621	0.595

TABLE 3—continued. C40-C41.

Streamline A

x	$10\delta_1$	$10^2\theta_{11}$	$10^3\theta_{12}$	$10^4\theta_{122}$	$10\delta_3$	$10^2\theta_3$	H_1	
9	0.32	1.18	-1.93	0.195	-0.42	0.211	1.37	1.537
10	0.34	1.25	-1.90	0.002	-0.23	0.221	1.46	1.516
11	0.37	1.33	-0.19	-0.162	-0.26	0.234	1.56	1.503
12	0.39	1.41	0.57	-0.309	-0.41	0.249	1.67	1.490
13	0.41	1.46	1.62	-0.435	-0.64	0.256	1.73	1.478
14	0.43	1.53	1.94	-0.547	-0.90	0.265	1.81	1.462
14	0.44	1.55	2.19	-0.592	-0.98	0.271	1.85	1.465
15	0.45	1.58	2.70	-0.685	-1.31	0.274	1.89	1.456
16	0.48	1.65	3.47	-0.838	-1.87	0.286	1.97	1.446
17	0.49	1.69	3.96	-0.901	-2.16	0.292	2.03	1.435
18	0.52	1.76	4.53	-1.026	-2.65	0.304	2.13	1.431
19	0.54	1.81	5.09	-1.090	-2.96	0.311	2.19	1.424
20	0.56	1.87	5.56	-1.179	-3.37	0.321	2.27	1.417
21	0.58	1.94	5.89	-1.242	-3.61	0.334	2.36	1.413
22	0.61	2.03	6.55	-1.397	-4.27	0.350	2.48	1.409
23	0.64	2.11	6.44	-1.393	-4.09	0.363	2.59	1.404
23	0.65	2.14	6.92	-1.410	-4.11	0.368	2.68	1.406
24	0.67	2.22	6.83	-1.455	-4.22	0.380	2.74	1.398
25	0.69	2.28	6.70	-1.405	-3.90	0.389	2.80	1.392
26	0.74	2.44	6.82	-1.407	-3.60	0.418	3.00	1.392
27	0.76	2.51	6.98	-1.407	-3.54	0.429	3.10	1.385
28	0.79	2.62	6.51	-1.358	-3.10	0.447	3.13	1.383
29	0.83	2.73	6.38	-1.341	-2.91	0.465	3.18	1.376
30	0.86	2.83	6.30	-1.314	-2.64	0.486	3.53	1.379
31	0.91	2.99	6.14	-1.275	-2.34	0.512	3.71	1.381
32	0.90	2.95	6.55	-1.359	-2.72	0.503	3.66	1.376
32	0.96	3.19	6.37	-1.313	-2.32	0.546	3.95	1.380
33	0.98	3.25	6.01	-1.235	-2.03	0.557	4.03	1.381
34	1.06	3.51	4.68	-0.971	-1.20	0.599	4.37	1.373
34	1.08	3.56	4.24	-0.920	-1.07	0.613	4.44	1.379
35	1.10	3.70	4.51	-0.962	-1.08	0.640	4.60	1.391
36	1.14	3.84	3.51	-0.720	-0.56	0.656	4.77	1.375
36	1.14	3.85	3.56	-0.773	-0.73	0.657	4.78	1.374
37	1.20	4.10	2.34	-0.265	-0.32	0.706	5.09	1.387
38	1.28	4.44	0.90	0.160	-0.31	0.769	5.51	1.396
39	1.50	5.27	2.58	-0.309	-0.36	0.948	6.57	1.444
40	1.66	5.88	4.96	2.31	-2.38	1.044	7.30	1.430
40	1.65	5.94	6.45	-2.456	-3.11	1.033	7.24	1.427
41	1.58	5.62	7.05	-3.216	-5.82	0.991	6.97	1.423
41	1.59	5.66	7.00	-3.17	-5.58	0.994	7.02	1.416
42	1.66	5.91	7.65	-3.582	-7.33	1.026	7.32	1.401
43	1.71	6.15	8.62	-3.685	-7.05	1.070	7.39	1.409
44	1.72	6.21	8.45	-3.367	-6.01	1.067	7.64	1.396
45	1.75	6.32	5.47	-2.605	-3.91	1.073	7.76	1.382

Streamline B

x	$10\delta_1$	$10^2\theta_{11}$	$10^3\theta_{12}$	$10^4\theta_{122}$	$10\delta_3$	$10^2\theta_3$	H_1	
9	0.29	1.03	-0.78	0.054	-0.12	0.185	1.19	1.559
10	0.31	1.10	0.04	-0.75	0.09	0.198	1.29	1.540
11	0.34	1.19	0.55	-0.233	-0.25	0.214	1.40	1.521
12	0.37	1.27	1.35	-0.400	-0.59	0.227	1.51	1.507
13	0.40	1.36	2.36	-0.603	-1.15	0.244	1.63	1.496
14	0.43	1.45	2.72	-0.675	-1.36	0.257	1.74	1.478
14	0.41	1.41	2.82	-0.672	-1.42	0.250	1.69	1.479
15	0.43	1.43	3.59	-0.752	-1.78	0.253	1.72	1.470
16	0.47	1.55	4.51	-0.949	-2.53	0.276	1.89	1.460
17	0.49	1.59	4.49	-0.965	-2.60	0.282	1.94	1.450
18	0.51	1.67	5.13	-1.061	-2.98	0.295	2.04	1.442
19	0.55	1.78	4.94	-1.094	-2.95	0.313	2.18	1.433
20	0.57	1.84	5.19	-1.120	-3.00	0.323	2.26	1.427
21	0.60	1.97	5.36	-1.174	-3.04	0.344	2.42	1.422
22	0.64	2.05	5.34	-1.175	-3.04	0.361	2.54	1.418
23	0.68	2.20	5.07	-1.148	-2.51	0.386	2.73	1.414
23	0.68	2.23	5.55	-2.445	-2.93	0.390	2.76	1.415
24	0.70	2.28	5.50	-2.108	-2.67	0.401	2.84	1.411
25	0.75	2.45	5.61	-2.140	-2.62	0.429	3.05	1.405
26	0.77	2.52	5.19	-2.173	-2.25	0.440	3.14	1.402
27	0.81	2.65	5.40	-1.214	-2.32	0.459	3.29	1.394
28	0.84	2.74	5.28	-1.157	-2.07	0.474	3.41	1.388
29	0.87	2.87	5.63	-1.168	-2.04	0.493	3.56	1.384
30	0.91	2.99	4.84	-1.012	-1.46	0.517	3.73	1.386
31	0.96	3.17	3.80	-0.837	-0.95	0.547	3.95	1.384
31	0.96	3.19	3.57	-0.724	-0.73	0.550	3.97	1.384
32	1.00	3.33	3.33	-0.643	-0.56	0.575	4.15	1.384
33	1.05	3.54	2.22	-0.364	-0.26	0.613	4.41	1.389
34	1.06	3.55	1.75	-0.336	-0.22	0.616	4.43	1.391
35	1.19	4.00	1.44	0.689	-0.58	0.690	4.99	1.382
36	1.29	4.44	3.19	1.352	-1.54	0.774	5.53	1.399
37	1.40	4.87	5.25	2.184	-3.17	0.858	6.06	1.417
38	1.75	6.43	9.17	3.561	-5.94	1.120	7.89	1.419
39	1.58	5.61	9.10	3.878	-7.95	0.995	6.97	1.429
40	1.69	5.99	9.61	4.242	-8.81	1.067	7.45	1.432
41	1.76	6.33	8.35	3.646	-6.42	1.111	7.83	1.420
41	1.71	6.20	8.36	3.573	-6.34	1.085	7.05	1.419
42	1.75	6.44	9.17	3.561	-5.94	1.120	7.89	1.419
43	1.61	5.82	9.01	2.859	-4.93	0.978	7.14	1.368
44	1.46	5.30	6.60	1.768	-2.52	0.853	6.36	1.343

Streamline C

x	$10\delta_1$	$10^2\theta_{11}$	$10^3\theta_{12}$	$10^4\theta_{122}$	$10\delta_3$	$10^2\theta_3$	H_1	
9	0.26	0.90	-0.103	-0.002	0.165	1.04	1.587	
10	0.28	0.95	-0.103	-0.010	0.176	1.12	1.568	
11	0.31	1.03	0.096	-0.020	0.187	1.21	1.550	
12	0.34	1.11	0.129	-0.040	0.203	1.33	1.530	
13	0.37	1.20	0.180	-0.064	0.219	1.45	1.515	
14	0.41	1.32	0.235	-0.112	0.239	1.60	1.496	
14	0.43	1.34	0.261	-0.146	0.245	1.64	1.495	
15	0.44	1.42	0.335	-0.177	0.288	1.74	1.481	
16	0.48	1.52	0.353	-0.186	0.295	1.87	1.468	
17	0.52	1.65	0.353	-0.175	0.297	2.04	1.458	
18	0.56	1.78	0.408	-0.128	0.319	2.21	1.446	
19	0.59	1.90	0.407	-0.136	0.340	2.36	1.441	
20	0.63	2.03	0.425	-0.163	0.362	2.52	1.433	
21	0.67	2.15	0.435	-0.152	0.382	2.68	1.425	
22	0.71	2.28	0.369	-0.137	0.406	2.85	1.422	
23	0.74	2.37	0.367	-0.129	0.419	2.97	1.413	
23	0.74	2.38	0.405	-0.125	0.420	2.97	1.413	
24	0.77	2.51	0.398	-0.138	0.442	3.14	1.409	
25	0.81	2.63	0.385	-0.117	0.462	3.29	1.404	
26	0.86	2.80	0.344	-0.096	0.495	3.51	1.410	
27	0.90	3.22	-0.743	-0.075	0.518	3.70	1.400	
28	0.92	3.03	-0.783	-0.079	0.529	3.79	1.397	
29	0.97	3.20	-0.622	-0.050	0.559	4.00	1.398	
30	1.03	3.45	-0.129	-0.012	0.607	4.31	1.407	
31	1.08	3.66	-0.111	-0.012	0.644	4.58	1.408	
31	1.09	3.66	-0.109	-0.012	0.644	4.58	1.406	
32	1.16	3.95	-0.057	0.020	0.696	4.94	1.410	
33	1.22	4.23	-0.230	0.121	-0.107	0.747	5.27	1.417
34	1.29	4.48	-0.423	1.837	-0.243	0.794	5.59	1.422
35	1.38	4.80	-0.559	2.443	-0.391	0.853	5.99	1.424
36	1.44	5.05	-1.053	3.634	-0.793	0.899	6.39	1.428
36	1.46	5.12	-1.016	3.806	-0.820	0.909	6.39	1.424
37	1.54	5.45	-1.137	4.603	-1.133	0.970	6.78	1.430
38	1.61	5.72	-1.531	5.806	-1.689	1.015	7.10	1.429
39	1.65	5.88	-1.388	5.399	-1.480	1.033	7.29	1.416
40	1.66	5.71	-1.165	4.162	-0.989	0.984	7.07	1.392
40	1.63	5.73	-1.097	3.912	-0.866	0.991	7.11	1.393
41	1.53	5.52	-0.959	2.874	-0.530	0.933	6.77	1.377

TABLE 4 a to c.

Table 4 Displacement and momentum thicknesses
in inches, and the ratio H_1

TABLE 5

Estimates of Skin-friction Coefficient.

Position x, y	$10^3 \times \frac{\tau_w}{\frac{1}{2} \rho_e u_e^2}$	Position x, y	$10^3 \times \frac{\tau_w}{\frac{1}{2} \rho_e u_e^2}$
18, 6	2.32	30, 8	2.03
18, 10	2.38	33, 8	1.90
			1.98
22, 6	2.18		
	2.19	35, 8	2.06
22, 8	2.31	35, 9	1.98
	2.32		
22, 10	2.25	39, 7	1.60
	2.27	39, 10	1.44
24, 8	2.19		1.52
28, 6	1.98	41, 7	1.80
	2.03	43, 7	2.02
28, 8	2.04		2.00
	2.04		

TABLE 6
Curvatures of Streamline and Orthogonals.

Distance from throat in	K_1 in $^{-1}$	K_2 from geometry in $^{-1}$	K_2 from pressures in $^{-1}$
11	-0.0219	-0.0147	-0.0168
12	-0.0224	-0.0148	-0.0169
13	-0.0225	-0.0146	-0.0168
14	-0.0222	-0.0144	-0.0158
15	-0.0211	-0.0135	-0.0138
16	-0.0190	-0.0115	-0.0117
17	-0.0165	-0.0095	-0.0100
18	-0.0135	-0.0078	-0.0079
19	-0.0102	-0.0063	-0.0059
20	-0.0074	-0.0050	-0.0040
21	-0.0049	-0.0041	-0.0027
22	-0.0028	-0.0033	-0.0015
23	-0.0012	-0.0022	-0.0008
24	-0.0000	-0.0014	-0.0004
25	-0.0005	-0.0006	-0.0002
26	-0.0012	0.0000	0.0000
27	-0.0015	0.0015	0.0002
28	-0.0012	0.0030	0.0005
29	0.0012	0.0045	0.0012
30	0.0035	0.0060	0.0030
31	0.0056	0.0074	0.0053
32	0.0080	0.0080	0.0075
33	0.0103	0.0098	0.0090
34	0.0122	0.0109	0.0099
35	0.0140	0.0116	0.0105
36	0.0155	0.0120	0.0107
37	0.0168	0.0115	0.0097
38	0.0183	0.0106	0.0076
39	0.0181	0.0095	0.0033
40	0.0112	0.0075	0.0020

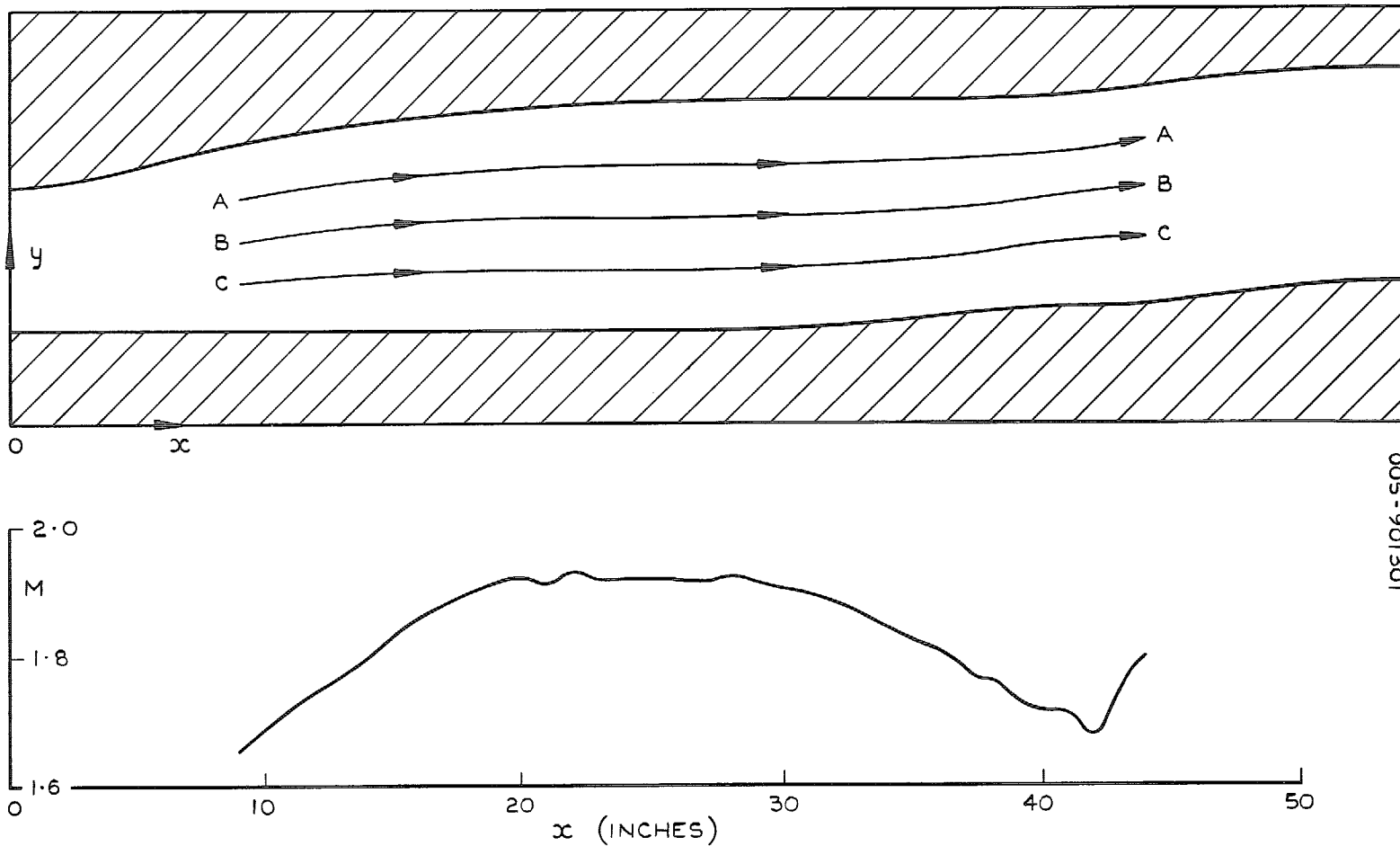


FIG. 1. External streamlines in test section. Mach number distribution along streamline B.

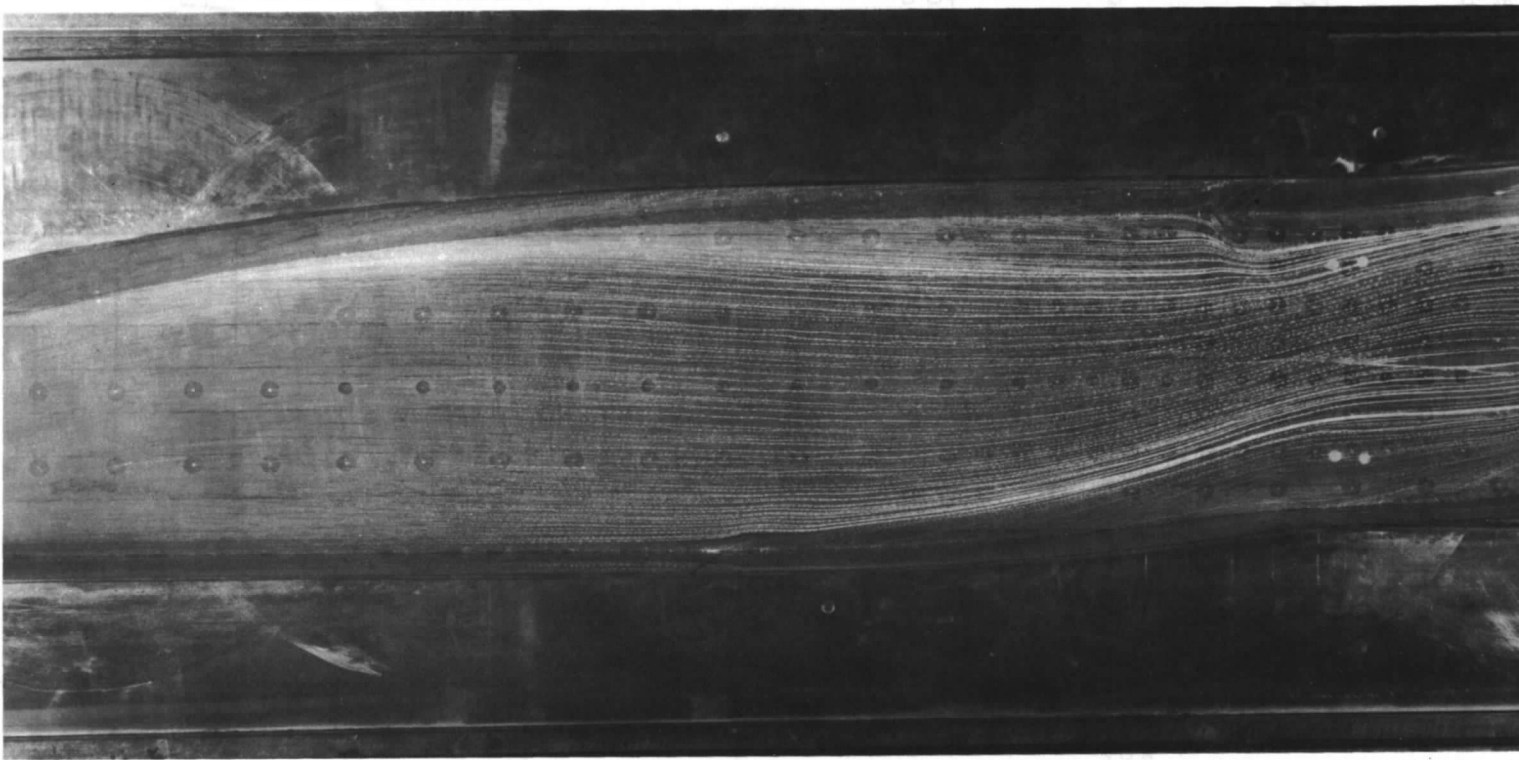


FIG. 2. Oil-flow pattern on wall showing limiting streamlines.

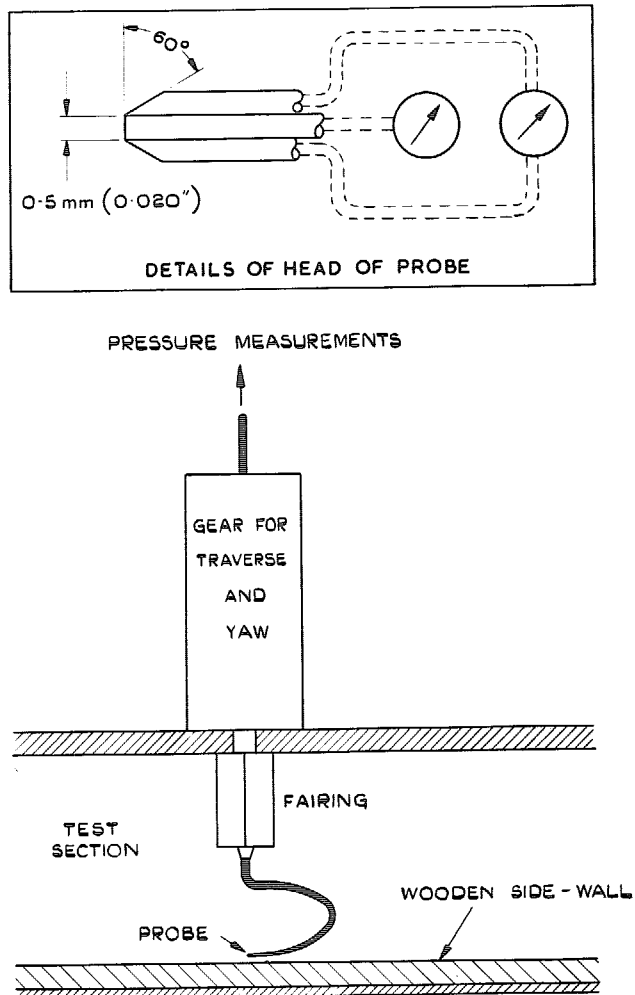


FIG. 3. Probe and traversing gear.

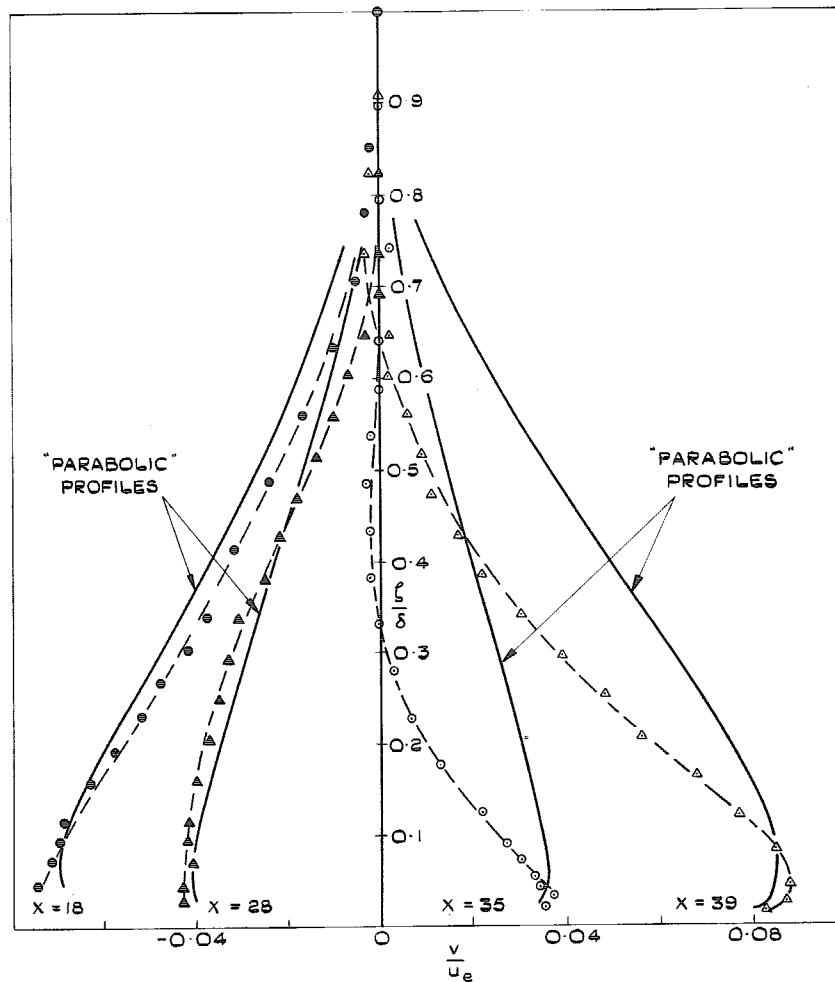


FIG. 4. Cross-flow profiles at stations x (inches)
Along streamline B.

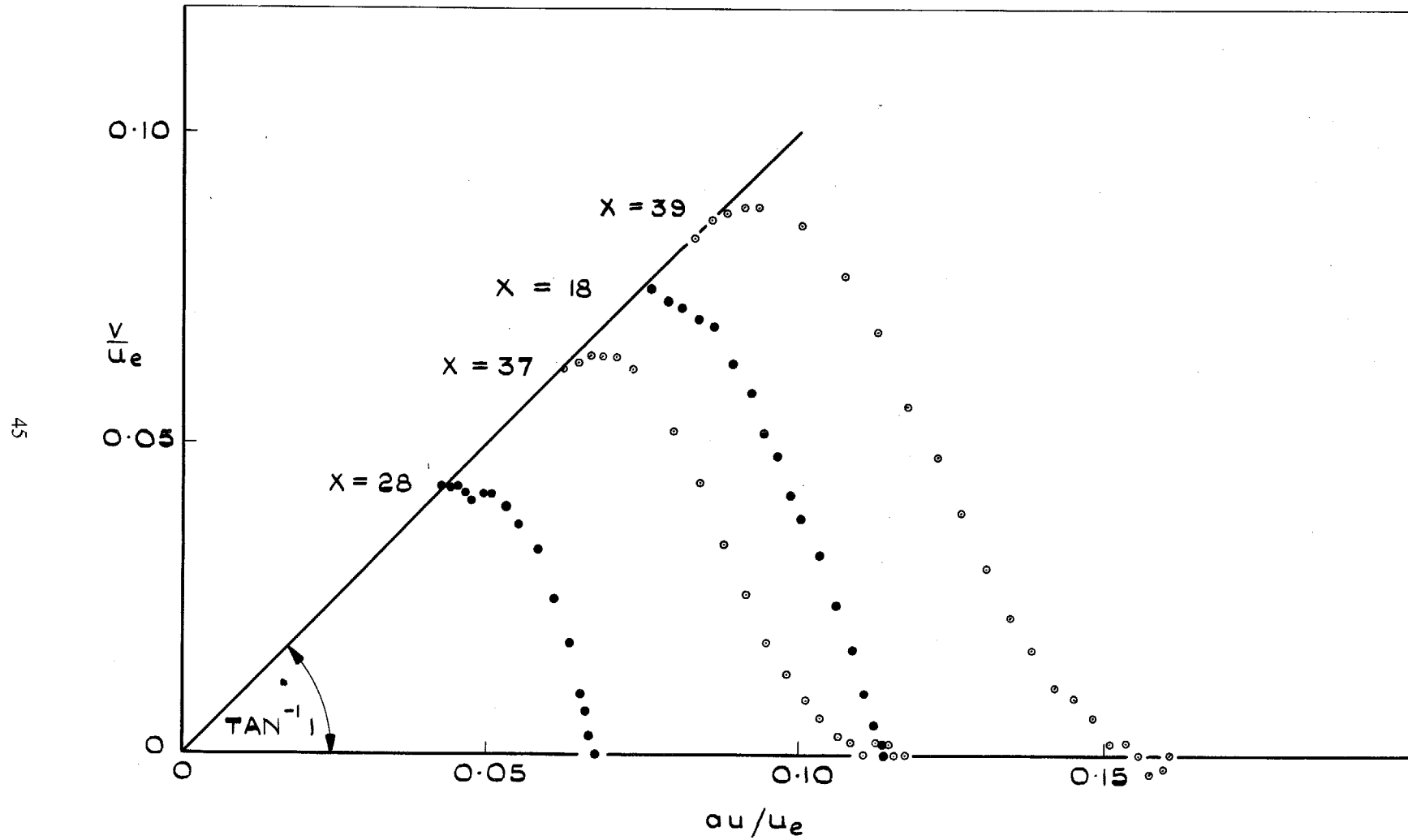


FIG. 5. Cross-flow profiles at stations x (inches) along streamline B—Polar plot.

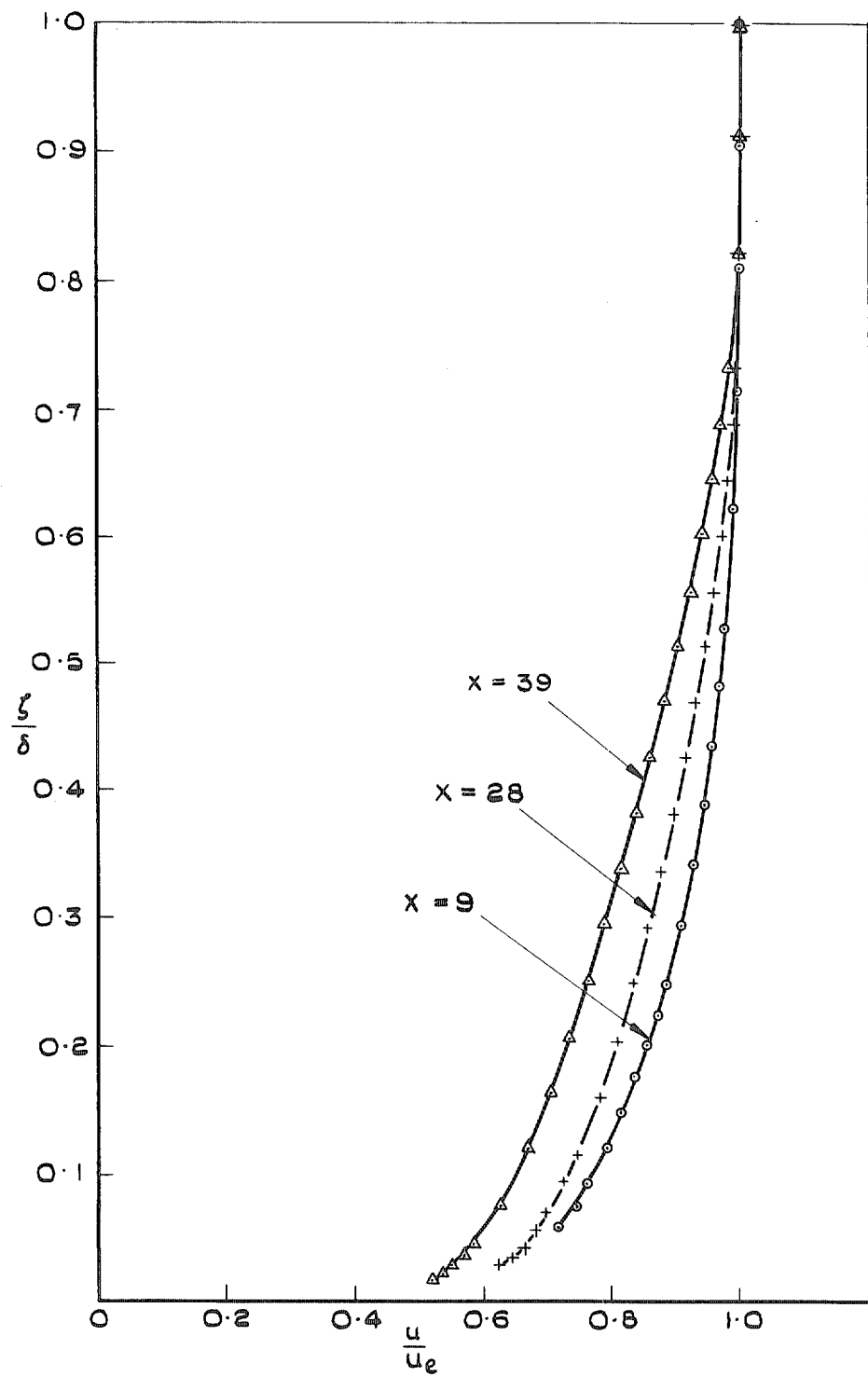


FIG. 6. Profiles of streamwise velocity component at stations x (inches) along streamline B.

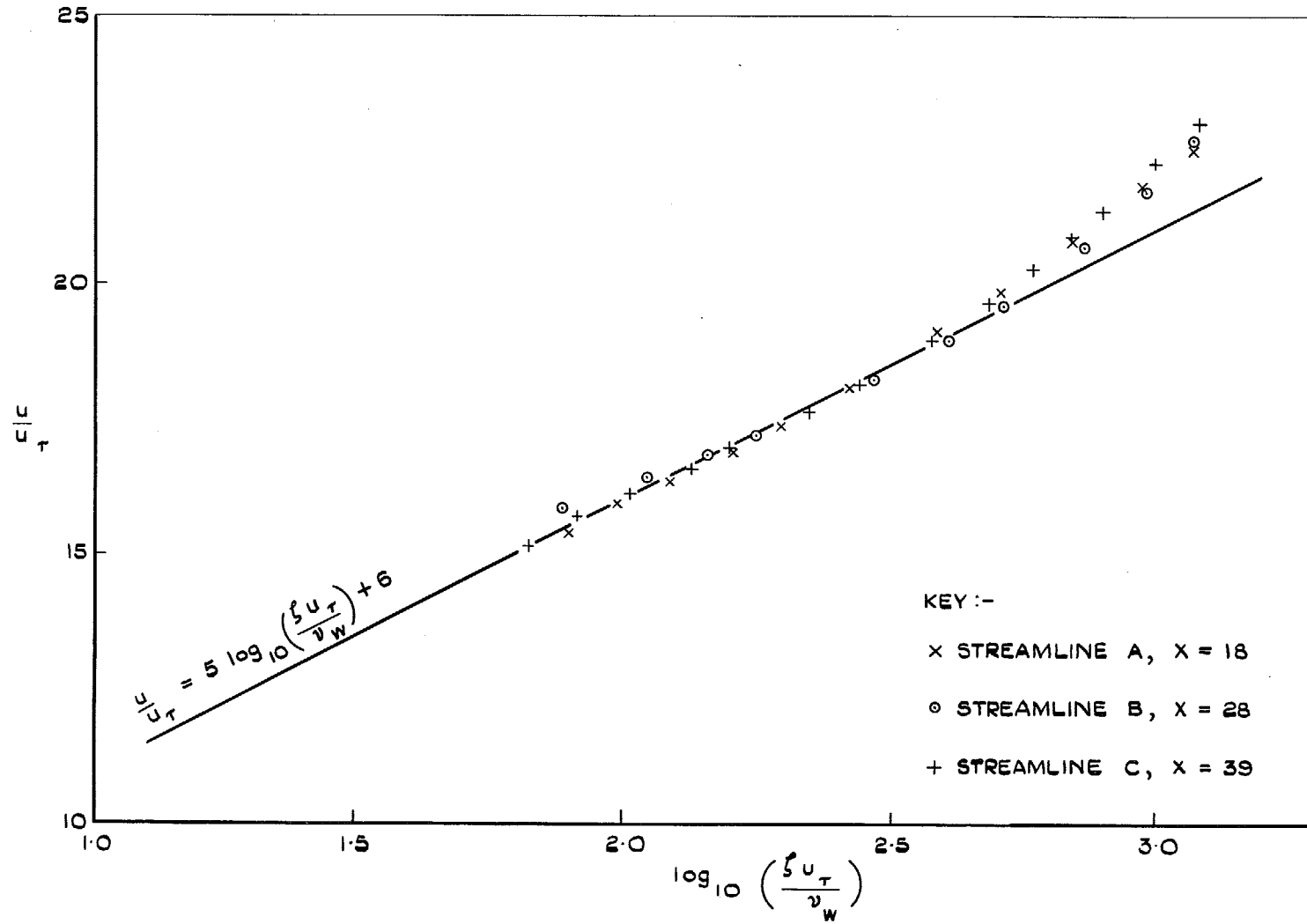


FIG. 7. Inner parts of profiles of streamwise velocity component—law of the wall.

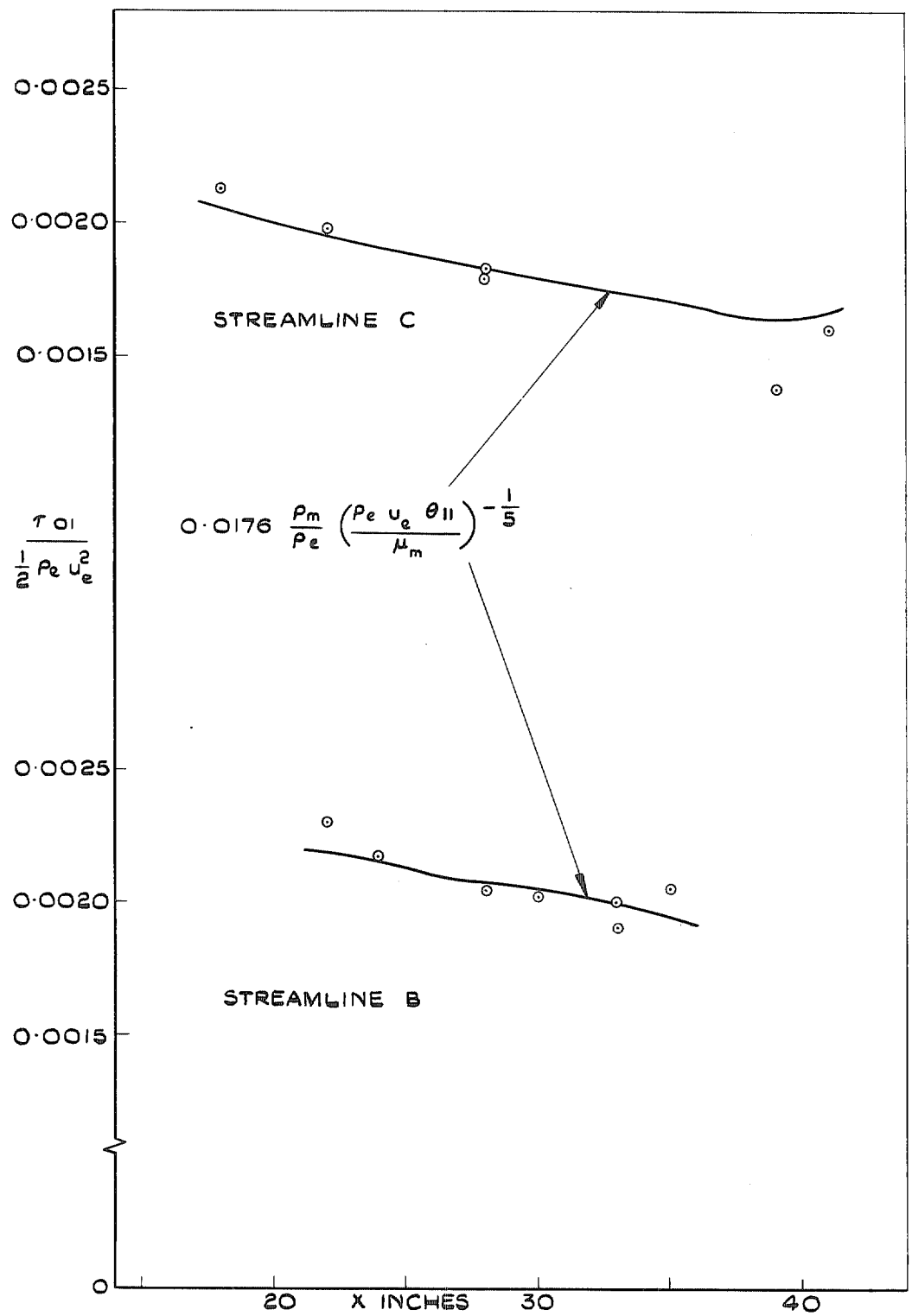


FIG. 8. Measured and estimated distributions of streamwise component of skin friction.

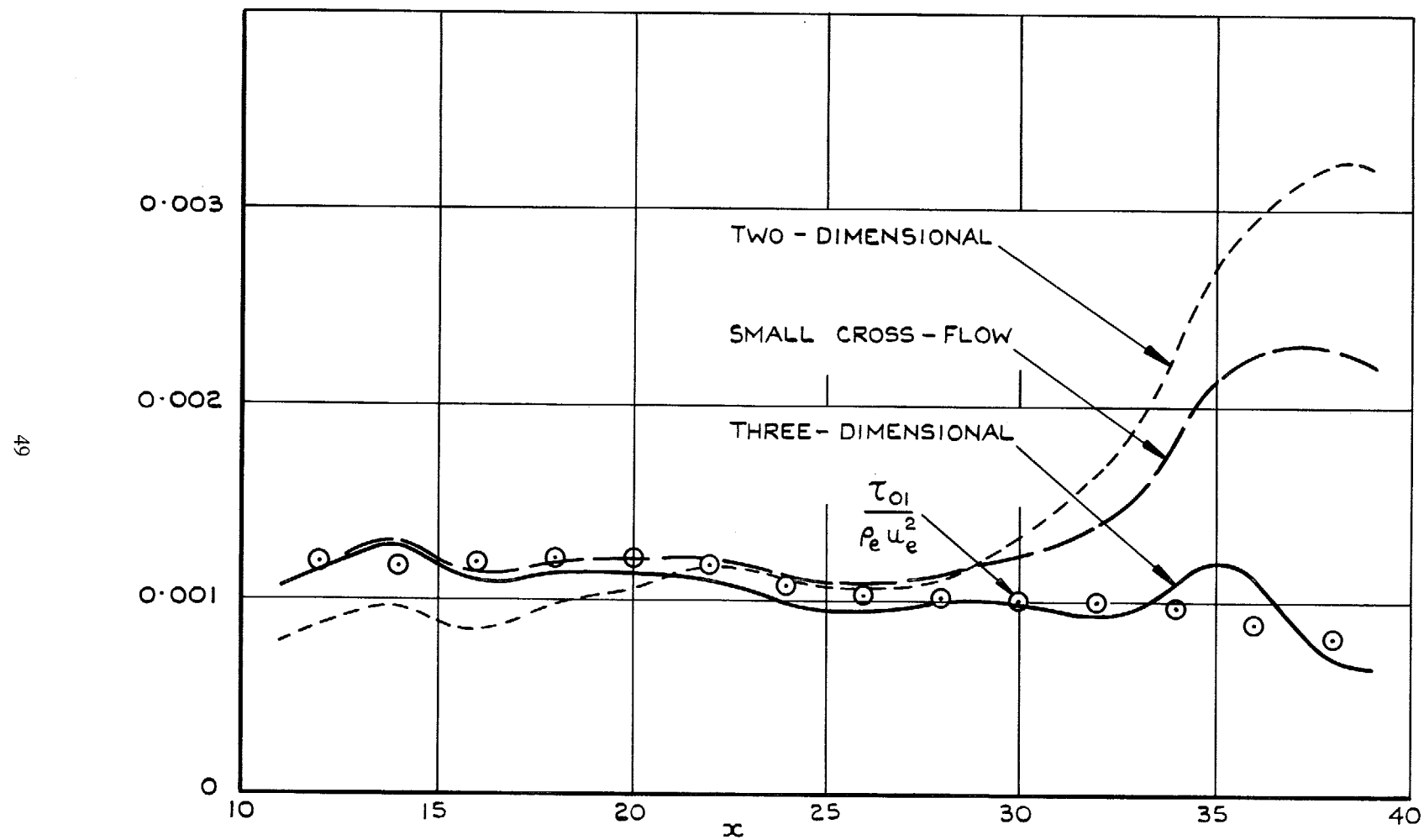


FIG. 9. Magnitudes of terms in streamwise momentum integral equation.

Printed in Wales for Her Majesty's Stationery Office by Allens Printers (Wales) Limited.

C Crown copyright 1968

Published by
HER MAJESTY'S STATIONERY OFFICE

To be purchased from
49 High Holborn, London w.c.1
423 Oxford Street, London w.1
13A Castle Street, Edinburgh 2
109 St. Mary Street, Cardiff c.11.1w
Brazennose Street, Manchester 2
50 Fairfax Street, Bristol 1
258-259 Broad Street, Birmingham 1
7-11 Linenhall Street, Belfast b12 8AY
or through any bookseller